METRICA
METRology Institutional CAtalog

ISTITUTO NAZIONALE DI RICERCA METROLOGICA
Repository Istituzionale

Validation report which details the advanced models developed to describe a) static and continuous and b) dynamic force transfer standards taking into account sensitivity stability,

Original
Validation report which details the advanced models developed to describe a) static and continuous and b) dynamic force transfer standards taking into account sensitivity stability, temperature and other parasitic influences on the measurement uncertainty (target uncertainty is 1 % up to 100 Hz and 2 % between 100 - 1000 Hz) / Sander, J.; Mirian, D.; Frank, H.; Hassan, S.; Kumme, R.; Prato, A.; Germak, A.; Wozniak, M.; Izquierdo, G.; Carmen, M.; Vavrecka, L.; Dizdar, H.; Aydemir, B.; Korhonen, J.; Oliveira, R. S.; Avila, M. - (2022), pp. 1-80. [10.5281/zenodo.7113187]
This version is available at: 11696/75840 since: 2023-02-17T17:21:10Z

Publisher:

Published
DOI:10.5281/zenodo.7113187

Terms of use:

This article is made available under terms and conditions as specified in the corresponding bibliographic description in the repository

Publication

Publisher copyright

(Article begins on next page)

12 October 2024

Part A
Static and continuous forces

EN

Static - Continuous

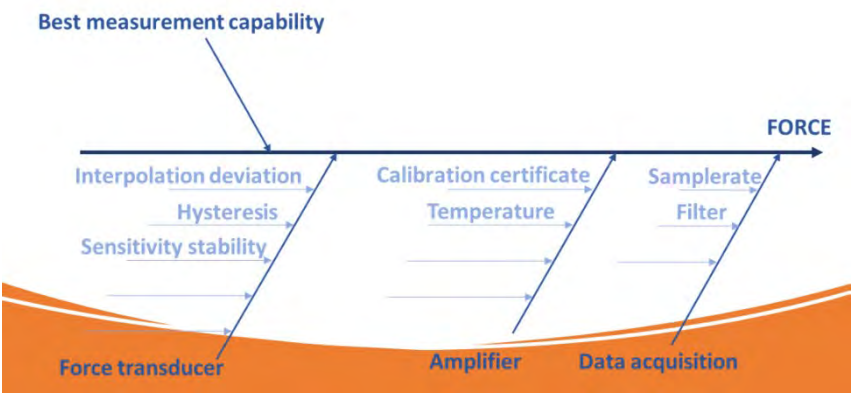

DOI: 10.5281/zenodo.7113187

Part A
Static and continuous forces

Version 1.0

Editors

Physikalisch Technische Bundesanstalt, Germany:
J. Sander, F. Hauschild, R. Kumme

CEM, Spain:
G. Izquierdo, M. Carmen

CMI, Czech Republic:
L. Vavrecka

INRiM, Italy:
A. Prato, A. Germak

Tubitak, Turkey:
H. Dizdar, B. Aydemir

VTT, Finland:
J. Korhonen

Inmetro, Brazil:
R. S. Oliveira

ZAG, Slovenia:
M. Hiti

Comprising the results from our research and the fruitful and intensive discussions with all our other project partners worldwide.

Contact: comtraforce@ptb.de

Braunschweig September 2022

DOI 10.5281/zenodo.7113187

Table of contents

Part A: Model static and continuous 7

1 Rheological Model 7

2 Static 8

2.1 Sensitivity: *9*

2.2 Sensitivity stability: *15*

2.3 Temperature: *15*

2.4 Tilt: *19*

2.5 Side forces: *19*

2.6 Bending moments: *21*

3 Continuous 23

3.1 Sensitivity: *23*

3.2 Creep / Relaxation: *28*

3.3 Temperature: *33*

3.4 Amplifier and data acquisition: *35*

4 Validation limits: 38

5 Practical model: 39

References 40

Part A: Model static and continuous

1 Rheological Model

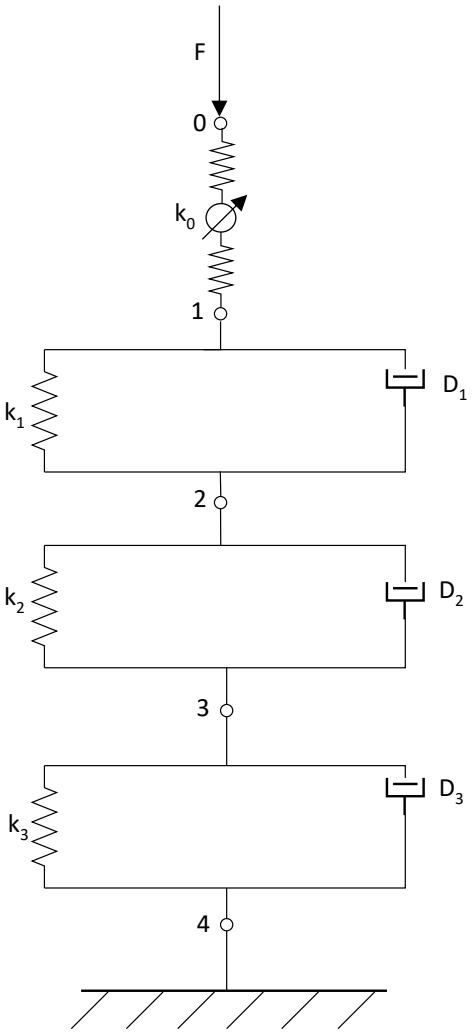

Figure 1 Generalized Kelvin model

A force transducer can be described for static and continuous forces with a rheological model consisting out of an (extended) Hooke element and N Kelvin-Voigt elements in series. For force transducers three Kelvin-Voigt elements are sufficient. This kind of assemble is called the generalized Kelvin model.

The displacement of point 0 relative to point 1 corresponds to the instantaneous output of the force transducer due to the application of a load step. The displacement of point 1 relative to point 4 corresponds to the creep / relaxation of the force transducer.

The elongation δ of the springs (Hooke element) in this model is defined by the following equation:

$$\delta = (1 - d(F)) \cdot \frac{F}{k} \tag{1}$$

In which F is the force acting on the spring and k is the stiffness constant of the spring. The damaging function $d(F)$ describes dependent on the applied force the non-linearity of the stiffness of the spring. The elongation of the dashpots is defined by an equation of the form

$$\frac{d\delta}{dt} = \frac{F}{D} \tag{2}$$

In which F is the force acting on the dashpot, t is the time variable, and D is the elongation-rate constant of the dashpot. The combination of a spring and a dashpot in parallel is called Kelvin-Voigt element. The spring and the dashpot experience in this combined element the same elongation and the sum of the forces acting on the spring and dashpot equals the force acting on the combined element. To simplify things, the function $d(F)$ in the spring element is here in the Kelvin-Voigt elements set to 0. The elongation of this element is thereby defined by a linear differential equation with constant coefficients of the form

$$D\frac{d\delta}{dt} + k\delta = F \tag{3}$$

Using the Boltzman superposition principle the elongation of the Kelvin-Voigt element is given by the following equation

$$\delta = \frac{F}{k}\left(1 - e^{-\frac{k}{D}t}\right) \tag{4}$$

The combination of all elements in series gives the total elongation due to a step loading function as following

$$\delta = (1 - d(F)) \cdot \frac{F}{k_0} + F\left[\left(\frac{1}{k_1} - \frac{1}{k_1}e^{-\frac{k_1}{D_1}t}\right) + \left(\frac{1}{k_2} - \frac{1}{k_2}e^{-\frac{k_2}{D_2}t}\right) + \left(\frac{1}{k_3} - \frac{1}{k_3}e^{-\frac{k_3}{D_3}t}\right)\right] \tag{5}$$

[1], [2], [3]

DOI 10.5281/zenodo.7113187

2 Static

For static force measurements it is assumed, that before the measurement value is taken the time-dependent creep / relaxation effects have already sufficiently subsided. The sensitivity is then only described by the elongation of the measured spring element due to a specific load step.

State of the art is the static calibration according to ISO 376 in which the force transducer is calibrated ideally in a deadweight force standard machine in steps from 10% to 100 % of the full-scale output (FSO) with dwell times of at least 30 seconds at each step. The measurement values are taken at the end of each step. This is done in three installation positions as it can be seen in Figure 2.

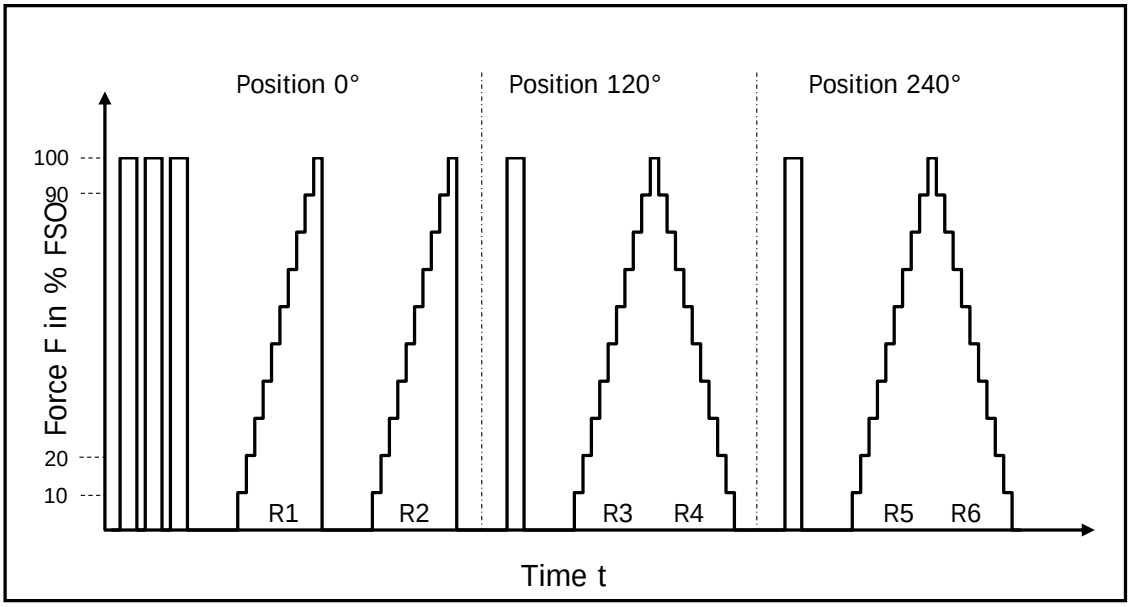

Figure 2 Measurement procedure according to ISO 376

At the end of the procedure a creep test is done in which the transducer is loaded with nominal load and held for 300 seconds. Values are taken at 30 seconds and 300 seconds after the full application of the load. Alternatively, this can also be done for the unloaded signal after the 300 second load step. This creep analyses is done to estimate the difference in creep between real static measurements and the calibration procedure. Further and more precise analyses are done in section 3 of this report.

[4]

2.1 Sensitivity:

For truly static measurements it can be assumed, that all time-dependent effects have already sufficiently subsided. In that case equation 5 can be simplified to the following equation

$$\delta = (1 - d(F)) \cdot \frac{F}{k_{static}} \quad (6)$$

$$with$$

$$k_{static} = \sum_{i=0}^{n} k_i$$

According to ISO 376 the sensitivity of a force transducer is given by the calibration function for increasing forces which is the indicated value as a function of the force which is fitted with a third-degree polynomial through the mean values of the measurement series R1, R3 and R5 (equation 7).

$$X_a = A \cdot F^3 + B \cdot F^2 + C \cdot F \quad (7)$$

With X_a as the balanced indicated value and A, B and C as the sensitivity coefficients.

A more practically and often used description of the sensitivity is the inverse function of the calibration function, which is the force as function of the indicated signal (equation 8).

$$F_{CD} = A' \cdot X_a^3 + B' \cdot X_a^2 + C' \cdot X_a \quad (8)$$

Investigation:

For this investigation the following force transducers were selected at PTB:

	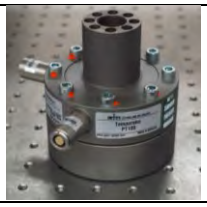		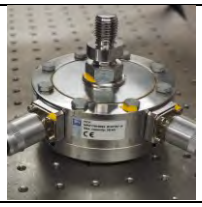	
Piezoelectric force transducer: **Type:** 9331B **Manufacturer:** Kistler **Nominal range:** 20 kN	Strain gauge transducer: **Type:** KTN **Manufacturer:** GTM **Principle:** Bending ring **Nominal range:** 25 kN	Strain gauge transducer: **Type:** Platinum 1810 **Manufacturer:** Interface **Principle:** Shear beam **Nominal range:** 25 kN	Strain gauge transducer: **Type:** U15 **Manufacturer:** HBM **Principle:** Shear beam **Nominal range:** 25 kN	Strain gauge transducer: **Type:** Dyn. Gen. 2 **Manufacturer:** Self-build by USTUTT, PTB and HBK **Principle:** Column **Nominal Range:** 20 kN

DOI 10.5281/zenodo.7113187

With the following amplifiers:

For strain gauge transducers:	For piezoelectric transducers
• Type: DMP 40 / DMP 41 • Manufacturer: HBM • Principle: Carrier-frequency • Resolution: 0.0000015 mV/V • Full range: 2.5 – 5 mV/V • Low-pass filter: 0.1 Hz Bessel	Charge amplifier: • Type: 5011b • Manufacturer: Kistler • Time constant: long DAQ: • Type: MGC Plus ML01 • Manufacturer: HBM • Resolution: 0.00001 V • Full range: 10 V • Low-pass filter: 0.1 Hz Bessel

All measurements were performed in tension and compression mode according to ISO 376 two times around six months apart on the deadweight 20 kN force standard machine (FSM) at PTB Braunschweig with a best measurement capability (bmc) of 0.002 %.

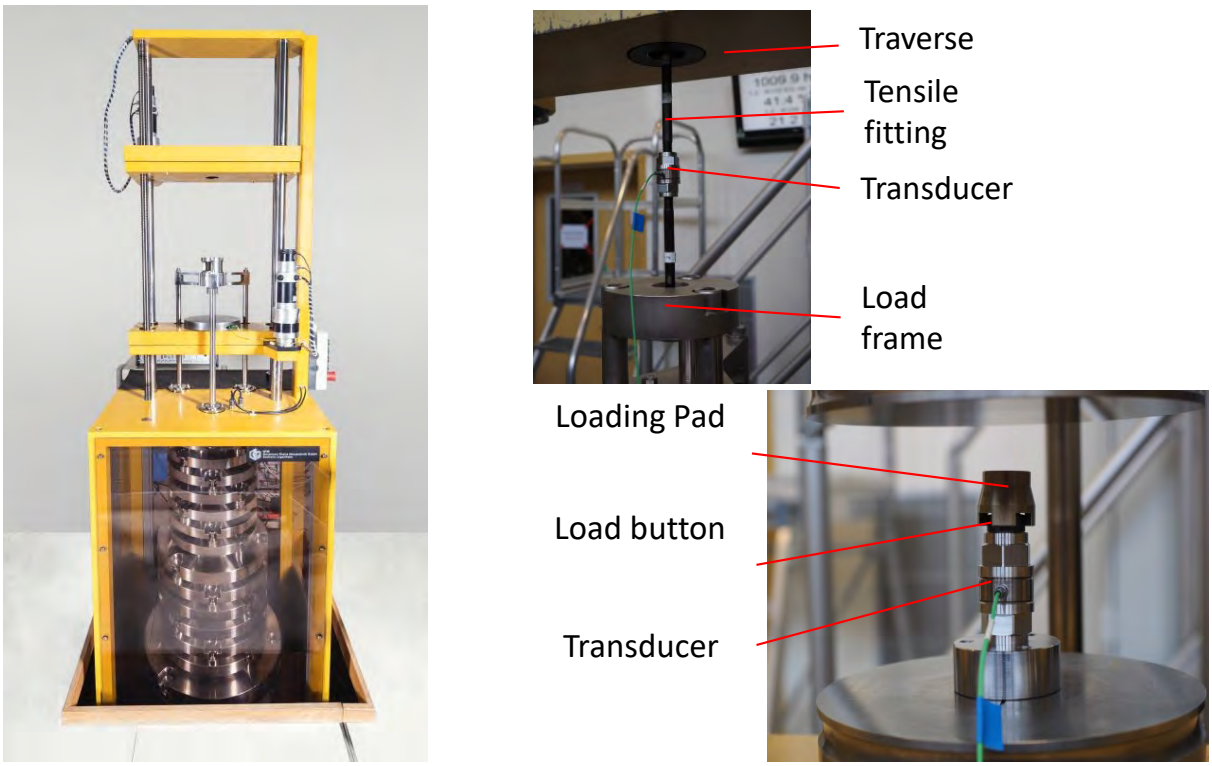

Figure 3 Deadweight 20 kN force standard machine (FSM) at PTB Braunschweig (left), typical mounting of the transducer for tension mode (upper right) and typical mounting of the transducer for compression mode (lower right)

Additionally, the GTM KTN was measured at CEM and the HBM U15 at CMI in compression mode.

Evaluation:

For the evaluation the calculation of the mean values was done after correction of the initial zero before each measurement series. After this a linear fit with no constant was executed within the Excel software. The deviation from this linear fit was then normalized to the maximum output and then plotted and fitted with a second-degree polynomial with no constant (intercept = 0) in the Origin software.

Results:

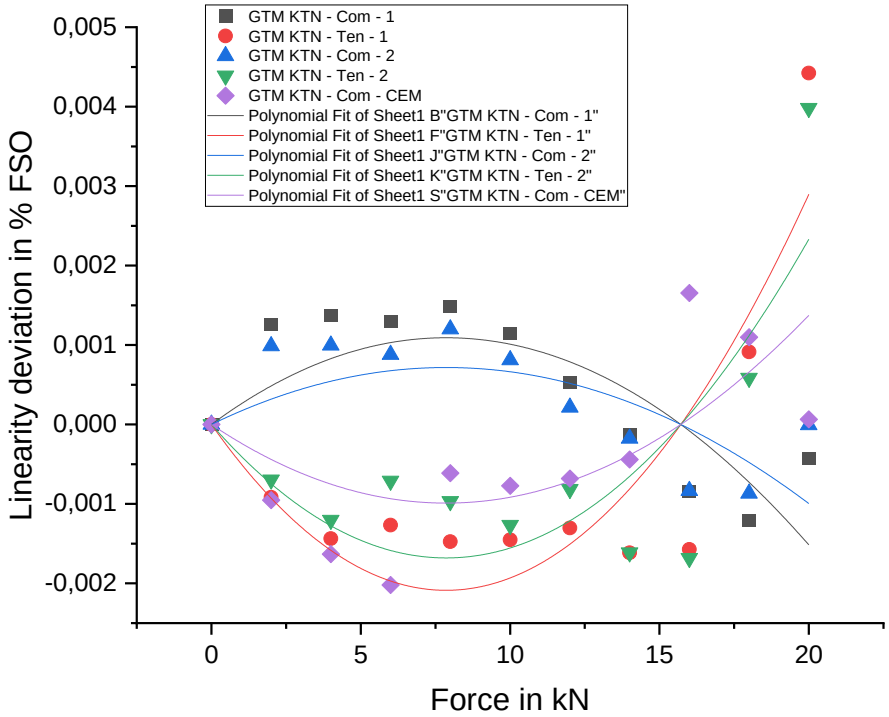

Figure 4 Static linearity deviation – GTM KTN in tension and compression modes (1 – first measurement / 2 – second measurement (6 months later))

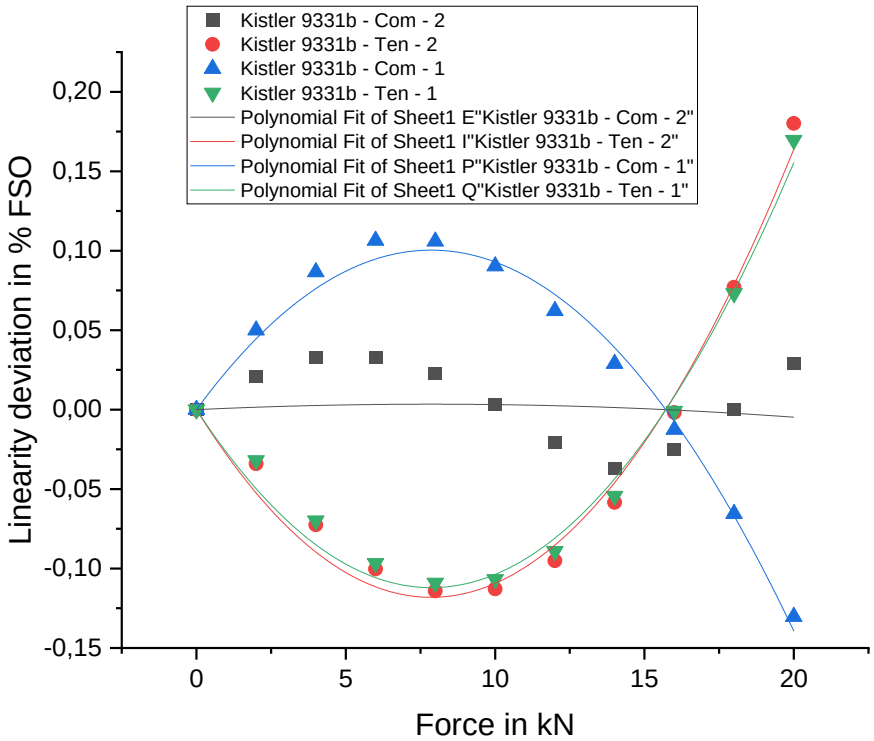

Figure 5 Static linearity deviation – Kistler 9331b in tension and compression modes (1 – first measurement / 2 – second measurement (6 months later))

DOI 10.5281/zenodo.7113187

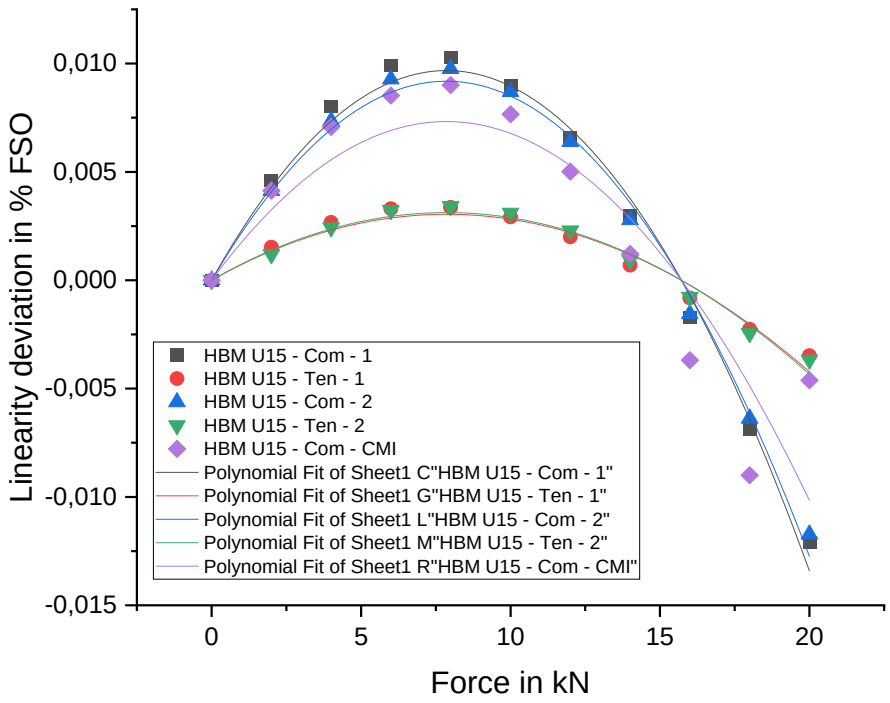

Figure 6 Static linearity deviation – HBM U15 in tension and compression modes (1 – first measurement / 2 – second measurement (6 months later))

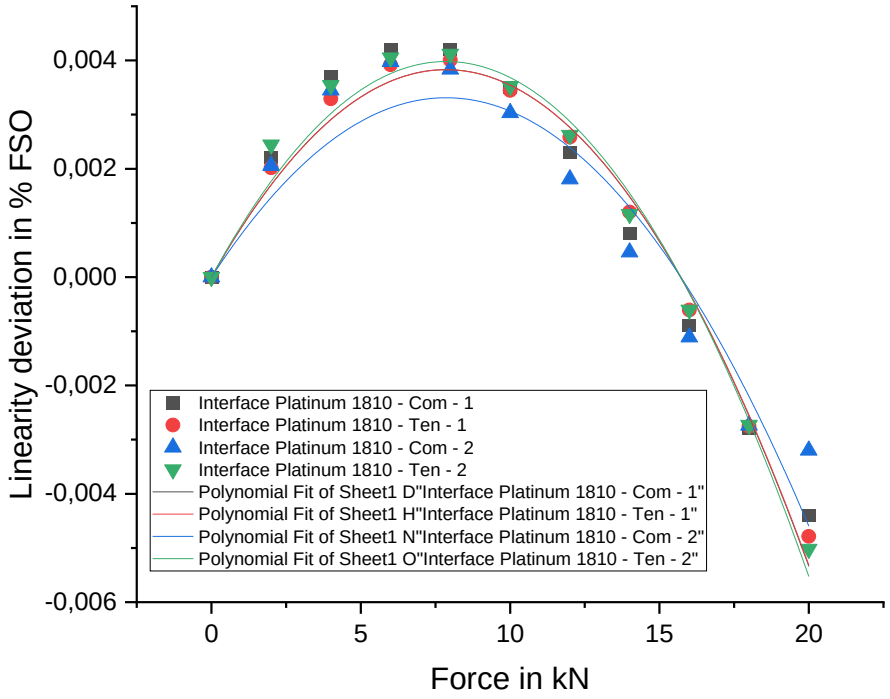

Figure 7 Static linearity deviation – Interface Platinum 1810 in tension and compression modes (1 – first measurement / 2 – second measurement (6 months later))

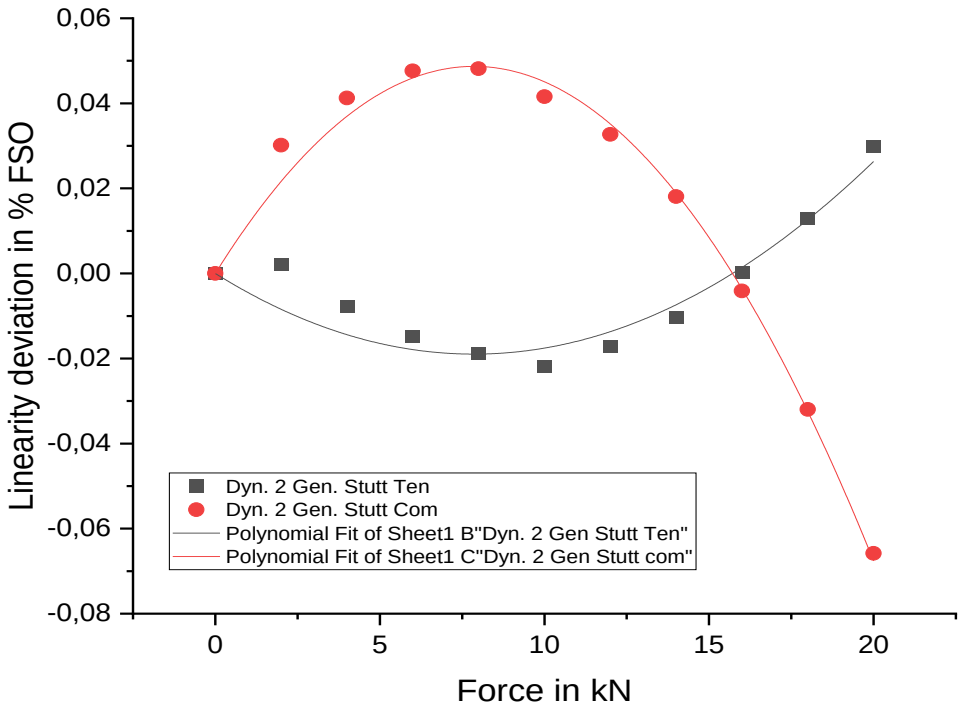

Figure 8 Static linearity deviation – Dynamometer 2. Generation Stutt in tension and compression modes

DOI 10.5281/zenodo.7113187

Table 1 Fitting parameters calculated by Origin Software of the second-degree polynomials to the linearity deviations of the transducers

Equation	y = Intercept + B1*x^1 + B2*x^2				
Plot	GTM KTN - Com - 1	GTM KTN - Ten - 1	GTM KTN - Com - 2	GTM KTN - Ten - 2	GTM KTN - Com - CEM
Weight	No Weighting				
Intercept	0 ± --	0 ± --	0 ± --	0 ± --	0 ± --
B1	2,77887E-4 ± 6,39061E-5	-5,31239E-4 ± 9,25689E-5	1,82486E-4 ± 5,91126E-5	-4,2754E-4 ± 1,00895E-4	-2,51851E-4 ± 8,90517E-5
B2	-1,76837E-5 ± 3,93912E-6	3,38061E-5 ± 5,70587E-6	-1,16128E-5 ± 3,64365E-6	2,72071E-5 ± 6,21907E-6	1,60269E-5 ± 5,48907E-6
Residual Sum of Squares	3,49716E-6	7,33772E-6	2,9922E-6	8,717E-6	6,7907E-6
R-Square (COD)	0,69129	0,79593	0,53022	0,68016	0,48645
Adj. R-Square	0,62269	0,75058	0,42582	0,60908	0,37233

Equation	y = Intercept + B1*x^1 + B2*x^2			
Plot	Kistler 9331b - Com - 2	Kistler 9331b - Ten - 2	Kistler 9331b - Com - 1	Kistler 9331b - Ten - 1
Weight	No Weighting			
Intercept	0 ± --	0 ± --	0 ± --	0 ± --
B1	8,74341E-4 ± 0,00272	-0,03006 ± 0,00128	0,02555 ± 8,56144E-4	-0,02851 ± 0,00114
B2	-5,56316E-5 ± 1,6744E-4	0,00191 ± 7,91271E-5	-0,00163 ± 5,27721E-5	0,00181 ± 7,03266E-5
Residual Sum of Squares	0,00632	0,00141	6,2766E-4	0,00111
R-Square (COD)	0,01212	0,98484	0,99061	0,98666
Adj. R-Square	-0,20741	0,98147	0,98852	0,98369

Equation	y = Intercept + B1*x^1 + B2*x^2				
Plot	HBM U15 - Com - 1	HBM U15 - Ten - 1	HBM U15 - Com - 2	HBM U15 - Ten - 2	HBM U15 - Com - CMI
Weight	No Weighting				
Intercept	0 ± --	0 ± --	0 ± --	0 ± --	0 ± --
B1	0,00246 ± 7,77831E-5	7,74574E-4 ± 4,45236E-5	0,00234 ± 6,34363E-5	7,94652E-4 ± 3,77148E-5	0,00186 ± 2,85266E-4
B2	-1,56654E-4 ± 4,79449E-6	-4,92911E-5 ± 2,7444E-6	-1,48737E-4 ± 3,91016E-6	-5,05687E-5 ± 2,32471E-6	-1,18609E-4 ± 1,75836E-5
Residual Sum of Squares	5,18086E-6	1,6975E-6	3,44592E-6	1,21802E-6	6,96837E-5
R-Square (COD)	0,99164	0,97286	0,99382	0,98133	0,83486

Equation	y = Intercept + B1*x^1 + B2*x^2			
Plot	Interface Platinum 1810 - Com - 1	Interface Platinum 1810 - Ten - 1	Interface Platinum 1810 - Com - 2	Interface Platinum 1810 - Ten - 2
Weight	No Weighting			
Intercept	0 ± --	0 ± --	0 ± --	0 ± --
B1	9,75685E-4 ± 6,23755E-5	9,74379E-4 ± 3,28918E-5	8,4275E-4 ± 8,52563E-5	0,00101 ± 4,08342E-5
B2	-6,21303E-5 ± 3,84478E-6	-6,20059E-5 ± 2,02743E-6	-5,36296E-5 ± 5,25513E-6	-6,44657E-5 ± 2,51699E-6
Residual Sum of Squares	3,33164E-6	9,26417E-7	6,22421E-6	1,42784E-6
R-Square (COD)	0,96668	0,99047	0,92046	0,98647
Adj. R-Square	0,95928	0,98835	0,90278	0,98346

Equation	y = Intercept + B1*x^1 + B2*x^2	
Plot	Dyn. 2 Gen Stutt Ten	Dyn. 2 Gen Stutt com
Weight	No Weighting	
Intercept	0 ± --	0 ± --
B1	-0,00483 ± 5,04309E-4	0,01239 ± 3,69487E-4
B2	3,07171E-4 ± 3,10852E-5	-7,88677E-4 ± 2,27749E-5
Residual Sum of Squares	2,17783E-4	1,16904E-4
R-Square (COD)	0,91561	0,99255
Adj. R-Square	0,89685	0,9909

Conclusion:

All transducers generally profited from a damaging function of a second-degree polynomial with no constant. So, a fitting of the sensitivity with a third-degree polynomial with no constant (equation 7) yields a good description. It is striking that for some transducers the linearity deviation is different between tension and compression modes. The linearity deviations were, except from the compression measurement of the Kistler 9331B transducer, repeatable.

The estimated sensitivity is though influenced by various parasitic components which need to be considered (Figure 8).

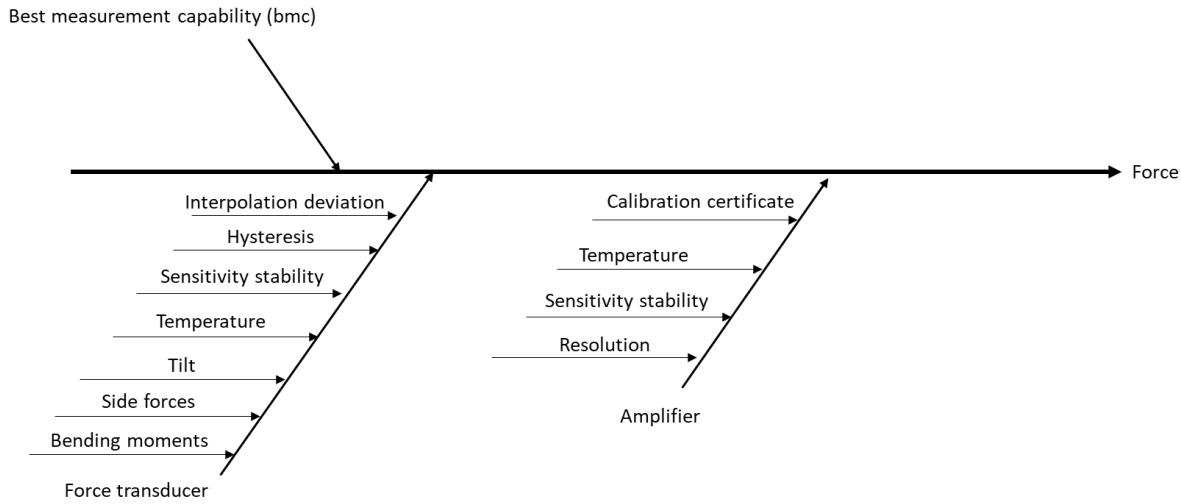

Figure 9 Ishikawa diagram of the influences on a statically calibrated force transducer

[4], [5], [6]

2.2 Sensitivity stability:

The stability of the sensitivity over a long time period (months and years) depends on the materials which were used for the transducer, the environment in which the transducer is used and the intensity of the usage of the transducer. That is why a model of this effect would not be generally representable for all transducers. That is why a transducer should be regularly calibrated to watch this effect and give based on these results an uncertainty for a certain time period.
[7]

2.3 Temperature:

In static measurements the temperature influences the zero-point stability and the sensitivity of strain gauge force transducers.

Investigation:

At PTB two different builds of the GTM KTN transducer were investigated. Both transducers are equipped with a PT100 for temperature measurements which are glued directly on the spring element next to the strain gauges of the transducers. As amplifier the DMP 40 from HBM was used. The measurements were performed at PTB with the 200 kN FSM with integrated temperature chamber.

The procedure consists of 18 cycles of increasing force steps (5 -10 – 15 – 20 kN) with waiting times of 360 seconds at each force step. This procedure was repeated with different temperatures (10 – 15 – 20 – 25 – 30°C)

DOI 10.5281/zenodo.7113187

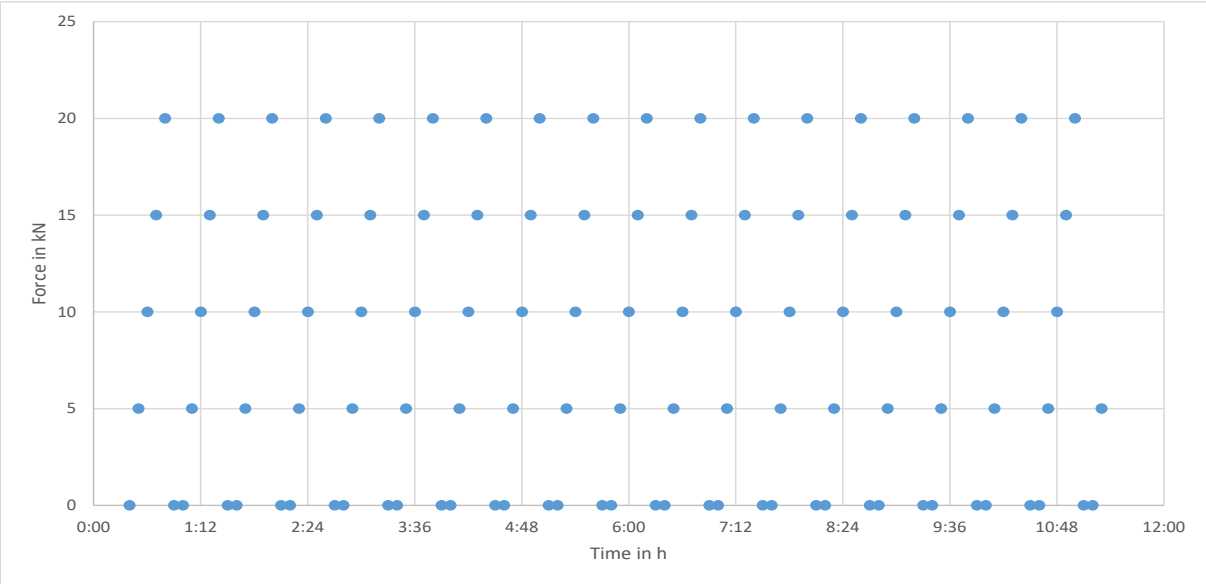

Figure 10 Measurement procedure at each temperature point for the estimation of the temperature dependency on sensitivity and zero point.

Evaluation:

For the evaluation of the temperature dependency of the sensitivity the mean values for each force level at each temperature are calculated after a correction of the initial zero before each cycle. For the evaluation of the temperature dependency of the zero point the first zero of the measurement procedure at each temperature is taken. To define the deviation of the zero due to temperature the zero at 20 °C was taken as the reference zero. The deviation from the reference zero is then normalized to the full-scale output (FSO).

Results:

Temperature on sensitivity:

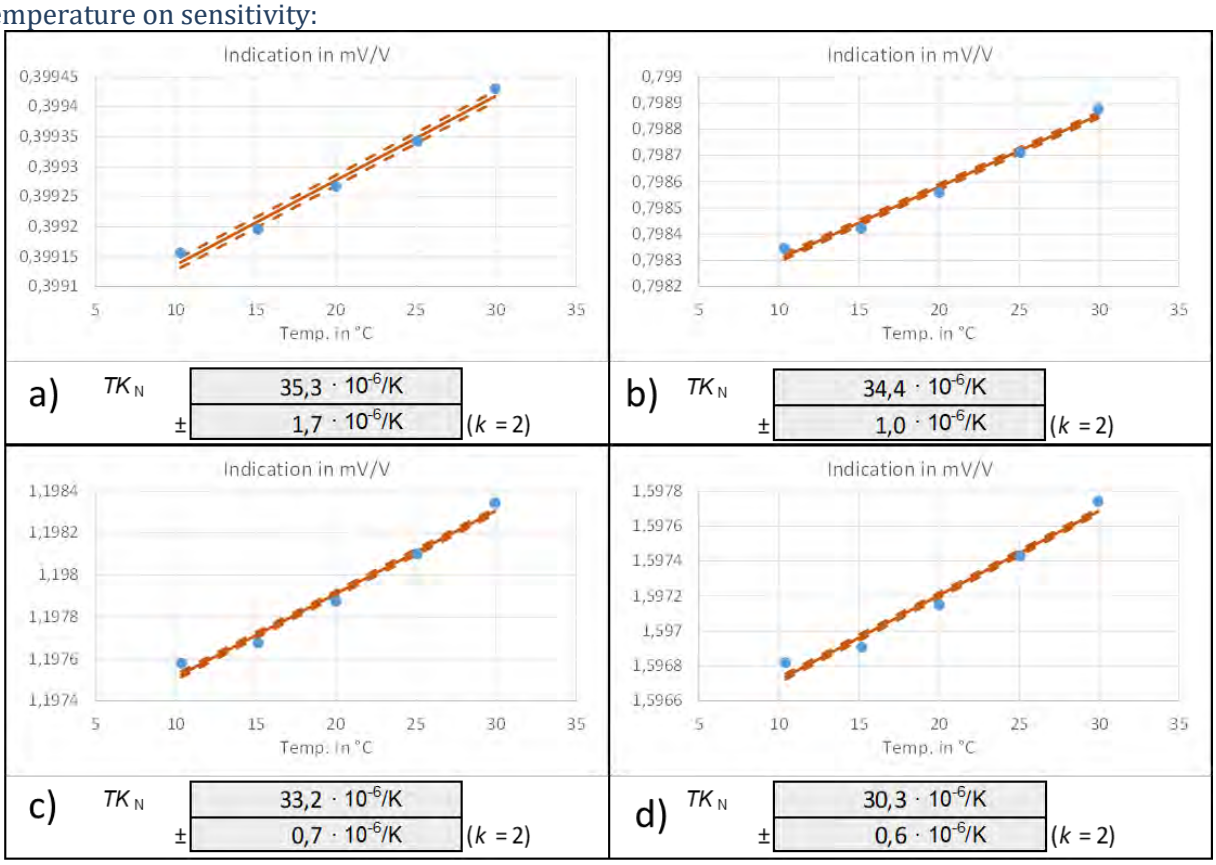

Figure 11 Temperature dependency of the sensitivity for GTM KTN 1 at PTB first measurement: a) 5 kN b) 10 kN c) 15 kN d) 20 kN

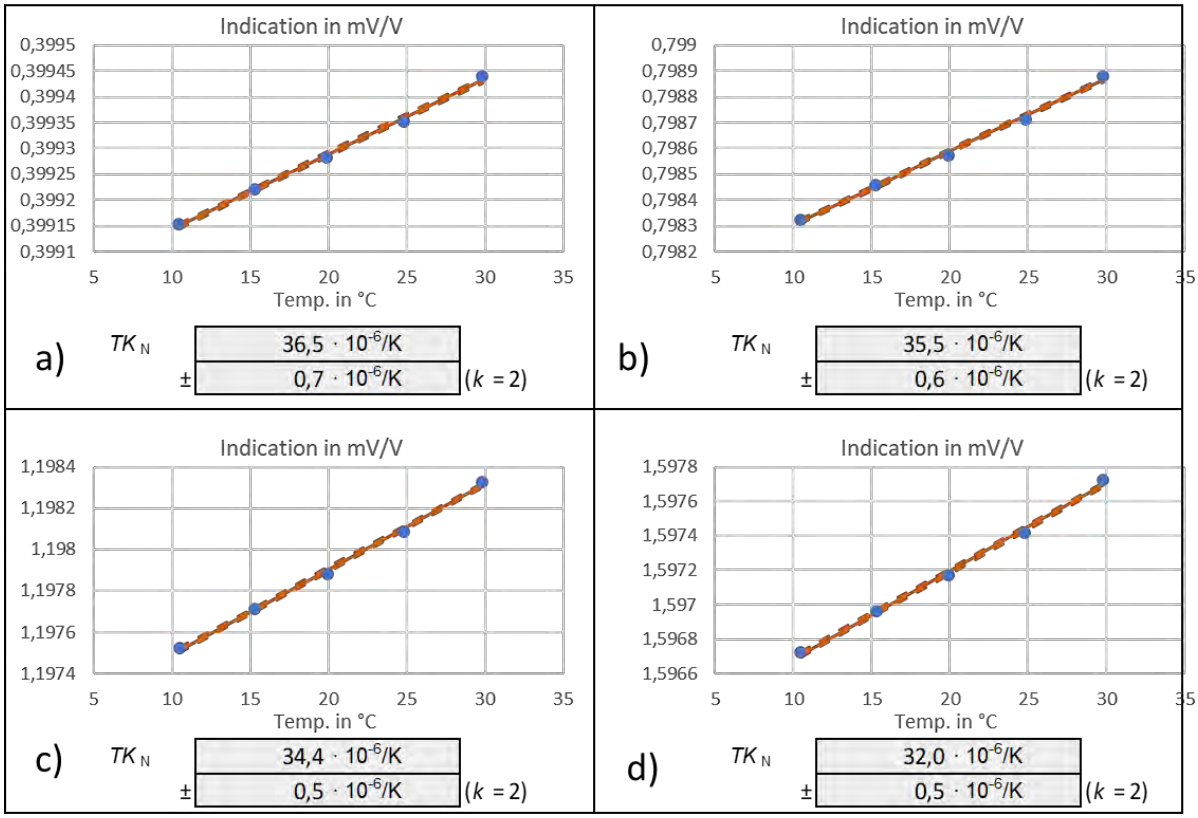

Figure 12 Temperature dependency of the sensitivity for GTM KTN 1 at PTB second measurement (1 year later): a) 5 kN b) 10 kN c) 15 kN d) 20 kN

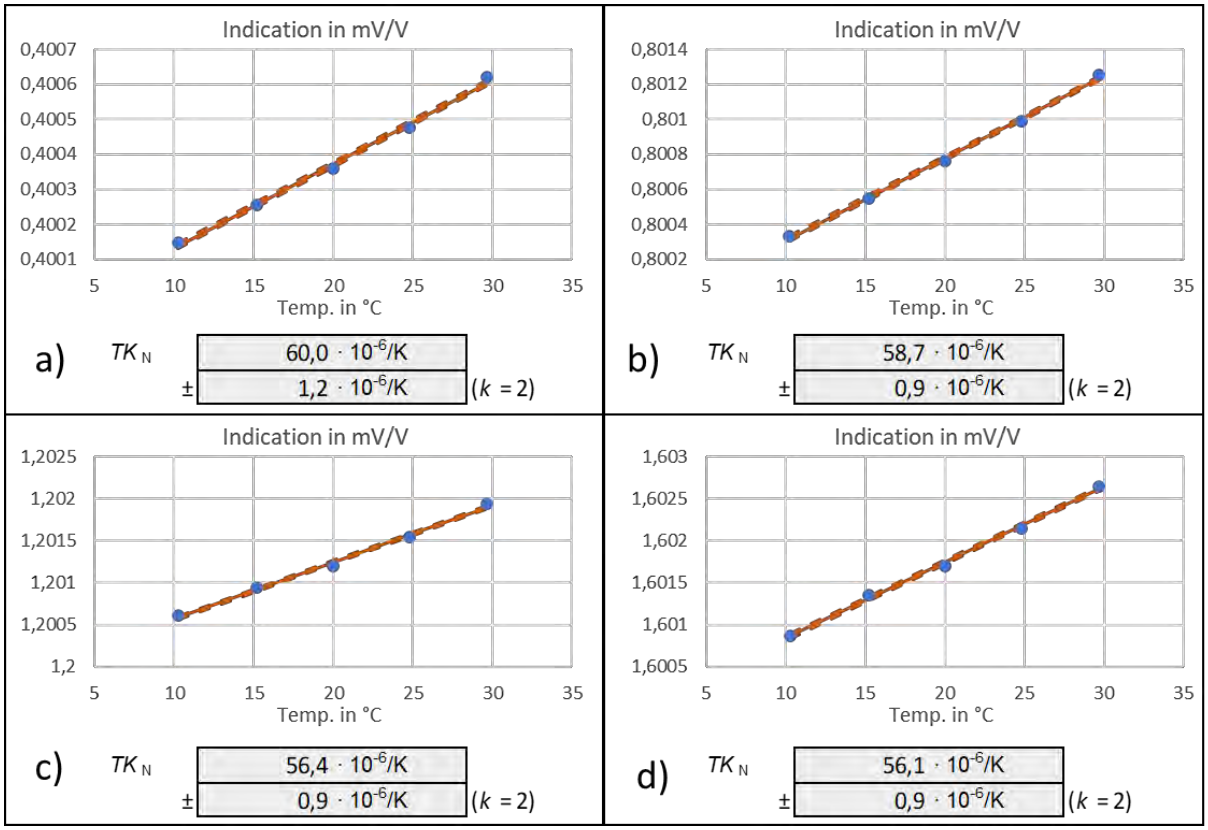

Figure 13 Temperature dependency of the sensitivity for GTM KTN 2 at PTB: a) 5 kN b) 10 kN c) 15 kN d) 20 kN

DOI 10.5281/zenodo.7113187

Temperature on zero point:

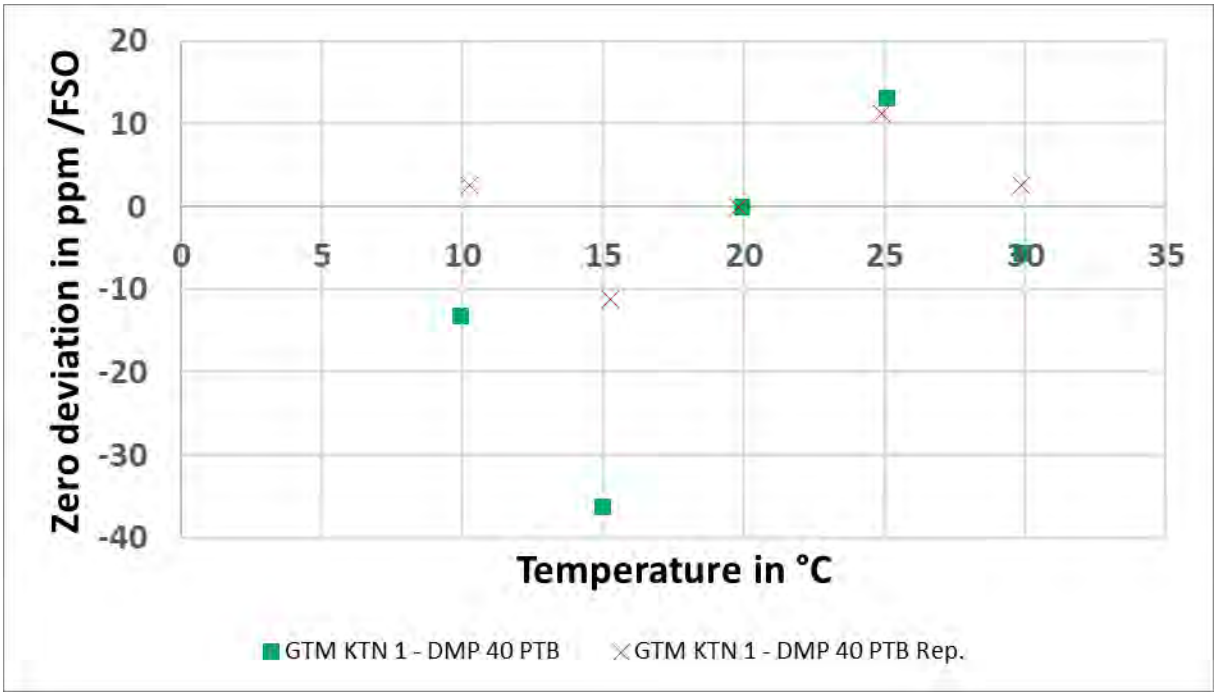

Figure 14 Zero point deviation due to temperature for the GTM KTN 1

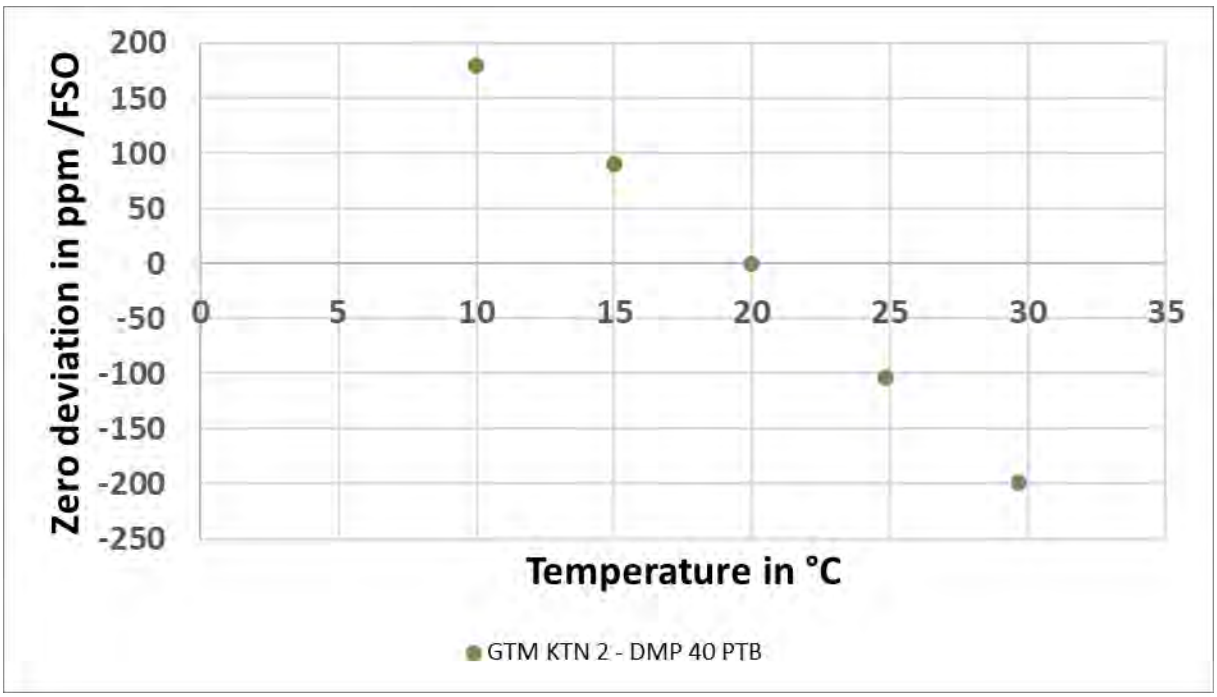

Figure 15 Zero point deviation due to temperature for the GTM KTN 2

Conclusion:

It could be shown, that the sensitivity is for the investigated transducers linear depend on the temperature in the range of 10 – 30 °C. It could be also observed that the zero point is dependent on temperature.
[8]

2.4 Tilt:

The not perfect verticality of the applied reference force, which means that the force is applied with an angle of tilt α with respect to the axis of the transducer under calibration, can be due to various factors that shall be evaluated by the calibration laboratory and depends on the type of machine. Such tilt angle α implies that the reference force F shall be multiplied by K_{tilt}=cos(α)~$(1-\frac{\alpha^2}{2})$ to get the force that is actually acting on the transducer F_{ref}. By performing the derivative of F_{ref} with respect to α, the sensitivity coefficient c_{tilt} used to propagate the uncertainty due to the tilt angle α is equal to sin(α)~α. Such tilt angles also produce spurious side forces, acting on the transducer under calibration and are proportional to sin(α). This contribution is described and analyzed in the next section.

2.5 Side forces:

The influence of spurious side forces F_s during the static calibration of uniaxial force transducers is evaluated at INRiM with two different deadweight force standard machines (FSMs), with a capacity of 30 kN (MCF30) and 1000 kN (MCF1000), respectively, both with a bmc of 0.002 %. Six different force transducers are tested with the same amplifier HBM DMP40:

Model	Capacity / kN	FSM
HBM Z3H3	5	MCF30
AEP KAL	10	MCF30
HBM Z3H3	20	MCF30
HBM Z4	100	MCF1000
HBM Z4	200	MCF1000
HBM C3H3	500	MCF1000

Known side forces are generated by integrating the FSMs with hardened steel tilted plates, between which the transducer under calibration is placed. By modulating the angle of tilt α, it is possible to decompose the applied reference force F generated by the FSM, with the result of generating vertical (see above) and side forces. Three couples of hardened steel (34CrNiMo6) tilted plates with angles of 1°, 2° and 3° are designed and manufactured to be installed in the deadweight FSMs at INRiM to generate the known side forces (see Figure 16).

Figure 16 The 20 kN transducer placed between the 3° tilted plates integrated into the MCF30 FSM

For each tilt angle (0° included), transducers are rotated around their axis with steps of 45° and three loads F (10 %, 50 % and 100 % of the transducers' capacity F_c) are applied. For each condition, the sensitivity, in (mV/V)/kN, is evaluated taking into account that the reference force acting on the transducer is given by

DOI 10.5281/zenodo.7113187

$F_{ref}=F\cos(\alpha)$. As an example, results, in terms of sensitivities evaluated with and without tilted plates as function of the rotation angle at a specific load of 50 % of the transducer's capacity, are shown in Figure 17 for the 5 kN transducer. Results with different tilted plates generating spurious side forces mainly follow a sinusoidal trend and the amplitude increases at increasing tilt angle (or increasing side force), so standard deviation does.

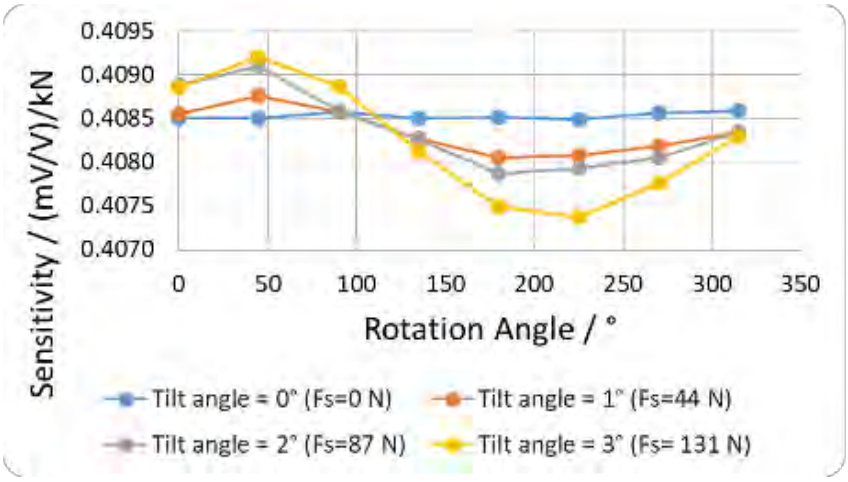

Figure 17 Sensitivity of the 5 kN transducer as function of the rotation angle with different spurious side force (or tilt angles) at an applied vertical force of 2.5 kN

Performing the mean sensitivity value from the eight rotations at different load conditions and the relative differences with respect to the reference condition without tilted plates, and plotting them as function of the side force F_s, it is found that the sensitivity decreases at increasing spurious side forces for each load condition for this specific transducer. This behaviour, however, varies from transducer to transducer. This means that the parasitic components influence the output of the transducers in a non-linear way, depending on their elastic sensitive element, the applied load and its direction. In general, relative sensitivity differences are in the order of 10^{-5} to 10^{-3}.

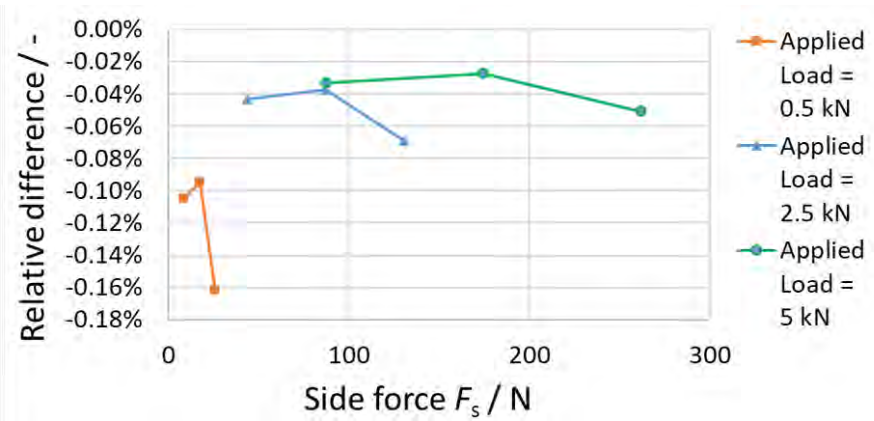

Figure 18 Relative differences of the 5 kN transducer as function of the side force at different applied loads

By performing a linear regression of the relative differences for all load conditions (i.e. 10 %, 50 % and 100 % of the transducer's capacity) and for each transducer, as function of the spurious side force F_s, the regression coefficients associated with side forces are found. These can be used as sensitivity coefficients to propagate the relative uncertainty of the transducer sensitivity associated with the side forces.

F_c / kN	Regression coefficient for side forces / N^{-1}
5	-2.37×10^{-5}
10	-1.34×10^{-7}
20	-1.35×10^{-8}
100	-1.84×10^{-7}
200	-8.86×10^{-8}
500	5.45×10^{-8}

Conclusion:

It is shown, that the sensitivity is influenced by spurious side forces F_s in the range of 9-17500 N for the investigated transducers with capacities from 5 kN to 500 kN.

2.6 Bending moments:

To evaluate the influence of spurious bending moments M_b, the same FSMs and force transducers used to evaluate the influence of side forces are selected, except for the 500 kN transducer. In this case, known spurious bending moments M_b are applied by misaligning the transducer with respect to the axis of the FSM. Three misalignments, without tilted plates in order to generate a pure bending moment, of 2 mm, 4 mm and 6 mm are applied to the transducers. For each misalignment, transducers are rotated around their axis with steps of 45° and three loads F (10 %, 50 % and 100 % of the transducers' capacity F_c) are applied. As an example, results, in terms of sensitivities evaluated with and without misalignments as function of the rotation angle at a specific load of 50 % of the transducer's capacity, are shown in Figure 13 for the 5 kN transducer.

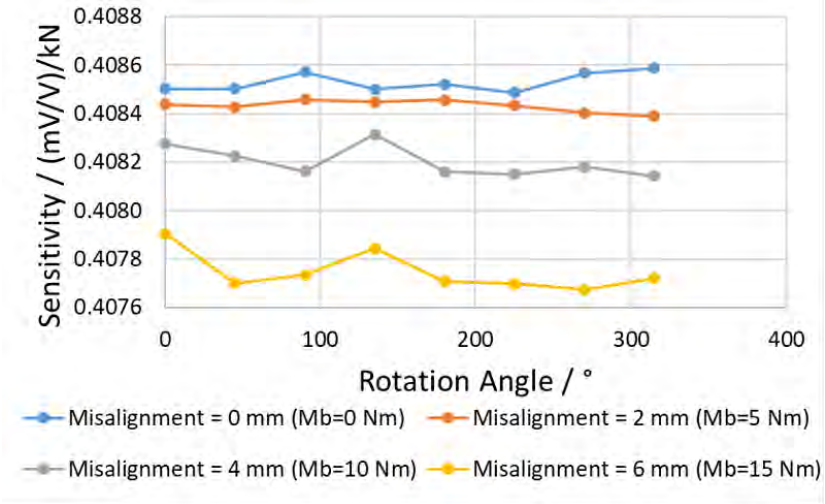

Figure 19 Sensitivity of the 5 kN transducer as function of the rotation angle with different spurious bending moments (or misalignments) at an applied vertical force of 2.5 kN

With different misalignments generating spurious bending moments M_b, standard deviations of the sensitivities are small and quite constant for different rotations. Similar behaviours are found for the other transducers. The mean sensitivity, however, decreases at increasing spurious bending moments for each load condition for this specific transducer. As for side forces, it is found that the sensitivity decreases at increasing spurious bending moments for each load condition for this specific transducer.

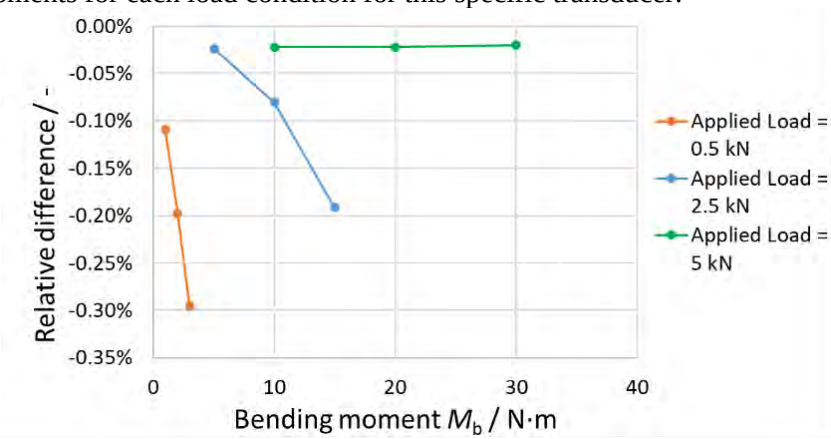

Figure 20 Relative differences of the 5 kN transducer as function of the bending moment at different applied loads

As for side forces, by performing a linear regression of the relative differences for all load conditions (i.e. 10 %, 50 % and 100 % of the transducer's capacity) and for each transducer, as function of the spurious bending moment M_b, the regression coefficients associated with bending moments M_b are found. These can be used as sensitivity coefficients to propagate the relative uncertainty of the transducer sensitivity associated with the bending moments M_b.

DOI 10.5281/zenodo.7113187

F_c / kN	Regression coefficient for bending moments / $(N\ m)^{-1}$
5	-3.71×10^{-4}
10	-1.02×10^{-4}
20	-4.61×10^{-5}
100	3.64×10^{-7}
200	-1.42×10^{-7}

Conclusion:

It is shown, that the sensitivity is influenced by spurious bending moments M_b in the range of 1-1200 N m for the investigated transducers with capacities from 5 kN to 200 kN.
[9], [10]

3 Continuous

In a continuous calibration a calibration device is calibrated mostly against a reference transducer in a machine which can apply a force continuously. Therefore, the reference transducer needs to be watched more closely in terms of time-dependent effects during its static calibration. A continuously variating force can be seen as infinitesimal force steps. Here equation 5 cannot be simplified like for the static measurements. To estimate the current sensitivity for a continuous force measurement the instantaneous sensitivity and the time dependent creep /relaxation behaviour needs to be measured separately. This can be done by performing fast loadings to estimate the instantaneous sensitivity and in addition to this by measuring the time-dependent creep / relaxation behaviour. One practical approach is the DKD 3-9 Annex 3.1 in which the results from a normal static calibration according to ISO 376 are compared to the results of a fast loading procedure.
[11]

3.1 Sensitivity:

For the description of the instantaneous sensitivity equation 5 simplifies to the following equation

$$\delta = (1 - d(F)) \cdot \frac{F}{k_0} \tag{9}$$

Here like in the static sensitivity description it is assumed that the damaging function can also be described with a second-degree polynomial resulting in a third-degree polynomial description of the instantaneous sensitivity (equation 10)

$$X_{a,instant} = R \cdot F^3 + S \cdot F^2 + T \cdot F \tag{10}$$

With R, S and T as sensitivity coefficients.

Investigation:

The same transducers as for the validation of the static sensitivity were used for this investigation. The same amplifiers, except for the Dynamometer, were used also. Although, the filter settings and the data acquisition needed to be changed. For the Dynamometer a DC amplifier was used.

DMP 40	DMP 41	MGC-Plus ML01	Dewetron DAQP STG (DC Amplifier)
Filter setting: 1.7 Hz Bessel Samplerate: 5 – 10 Hz	Filter setting: 2.0 Hz Bessel Samplerate: 5 – 10 Hz	Filter setting: 2.5 Hz Bessel Samplerate: 10 Hz	Filter Setting: 300 kHz Samplerate: 1000 Hz

The transducer is loaded in jumps directly from zero to the respective force level (Figure 20). The waiting time between the full application of the force (S3) and the measurement point (S4) is dependent on the machine and used filter setting of the amplifier. Only when both influences have sufficiently subsided the measurement value can be estimated. For the lowest filter (1.7 Hz Bessel) this lasted 3.5 seconds and for the highest filter (300 kHz) this lasted 0.3 seconds. Also of great importance is the loading time between S2 and S3. At PTB the maximum loading time lasted 2.3 seconds

DOI 10.5281/zenodo.7113187

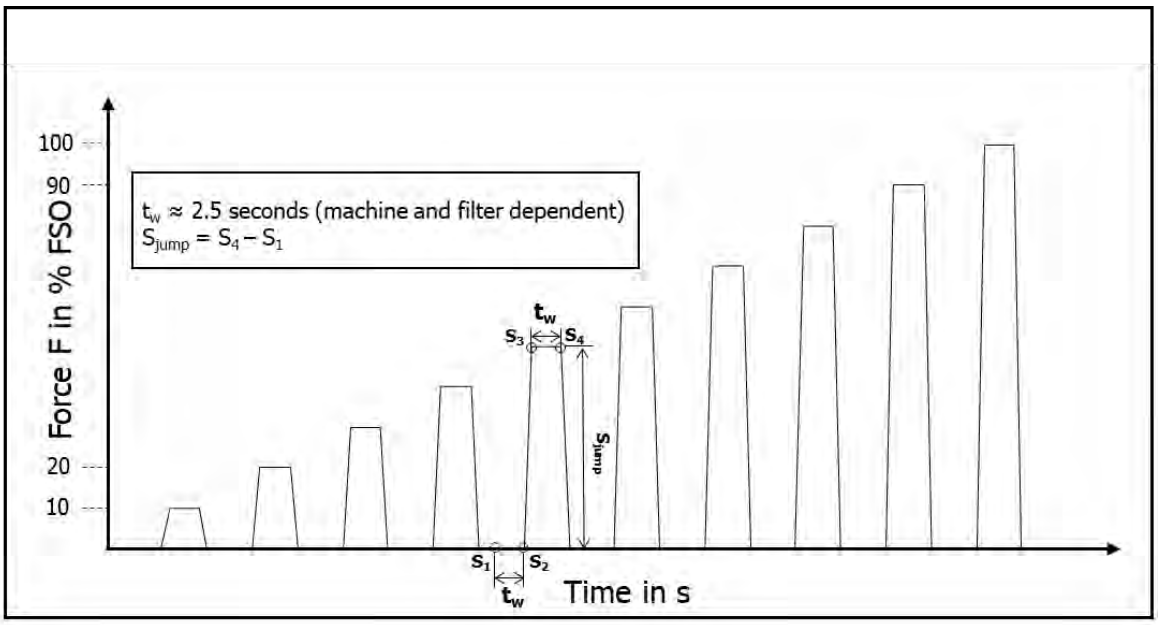

Figure 21 Procedure for estimating the instantaneous sensitivity

Evaluation:

For the evaluation of the measurement results the Excel software was used. Because of the higher filter settings as for the static measurements S4 was estimated by averaging by a few nearby points. After correction of the initial zero before each measurement series a linear fit with no constant was executed within the Excel software. The deviation from this linear fit was then normalized to the maximum output and then plotted and fitted with a second-degree polynomial with no constant in the Origin software.

Results:

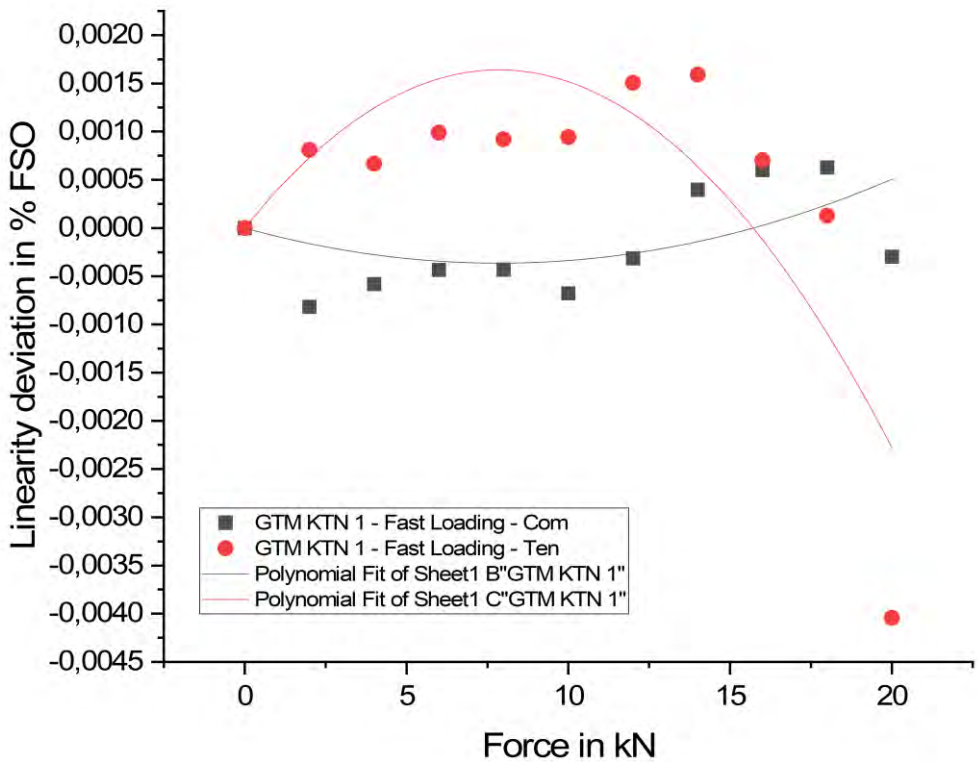

Figure 22 Instantaneous linearity deviation – GTM KTN 1 in tension and compression mode

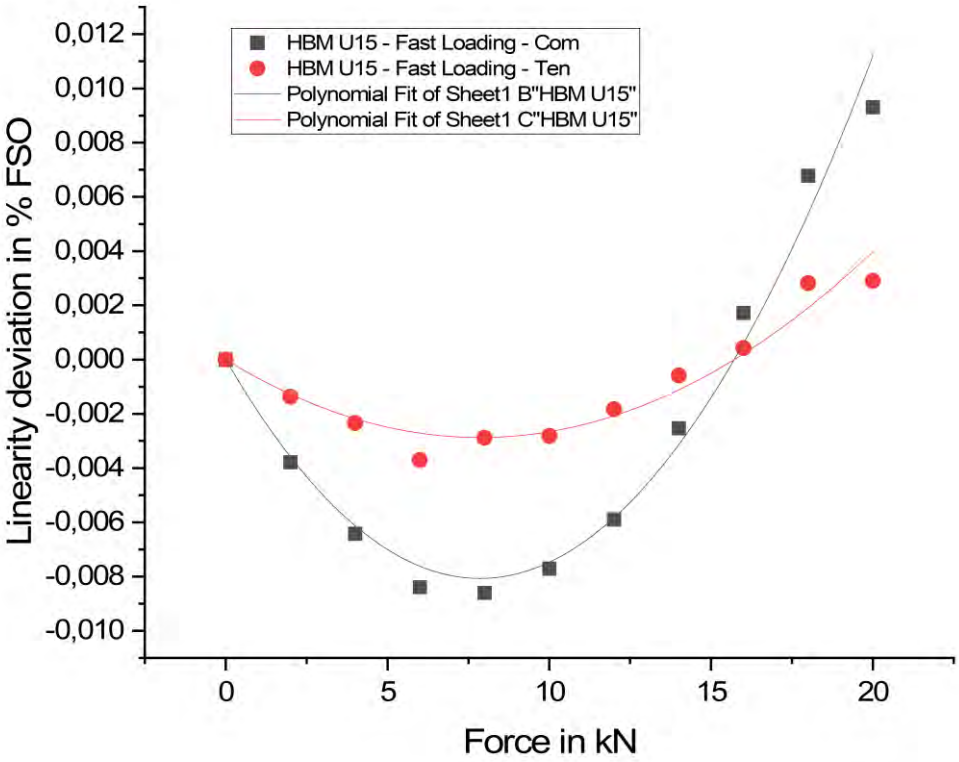

Figure 23 Instantaneous linearity deviation – HBM U15 in tension and compression mode

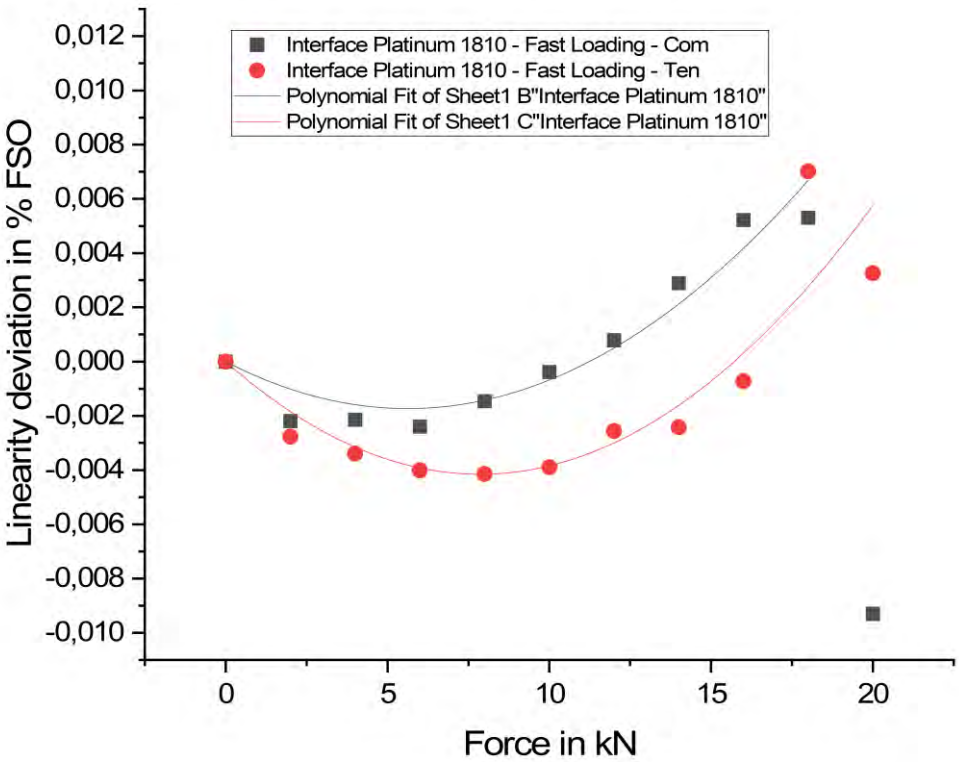

Figure 24 Instantaneous linearity deviation – Interface Platinum 1810 in tension and compression mode

DOI 10.5281/zenodo.7113187

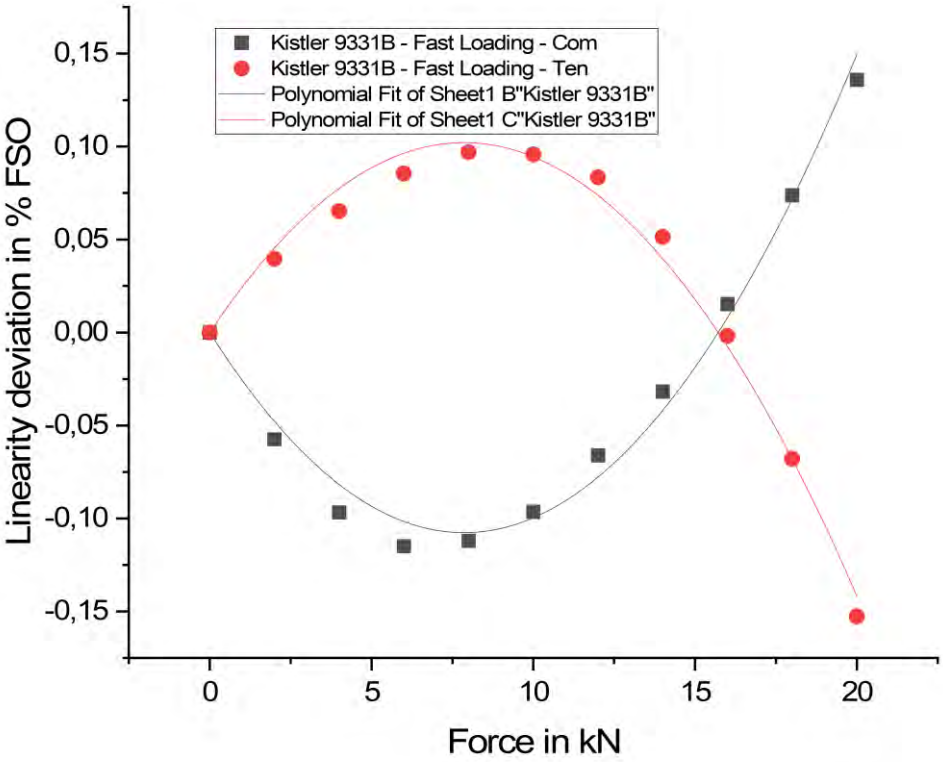

Figure 25 Instantaneous linearity deviation – Kistler 9331b in tension and compression mode

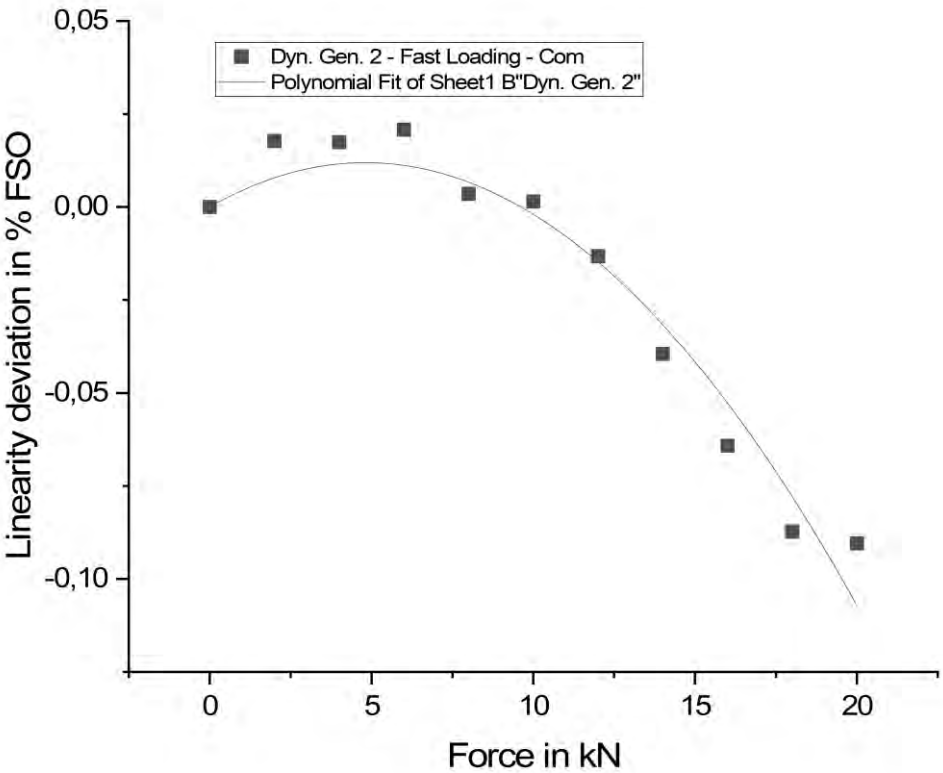

Figure 26 Instantaneous linearity deviation – Dynamometer 2. Generation Stutt in compression mode

Conclusion:
The linearity deviation measured with fast loadings can also be well described with a second-degree polynomial. That is why the instantaneous sensitivity can also be described with a third-degree polynomial. Similar to the static description influences on the sensitivity need to be incorporated (Figure 27). In addition to the influences for static forces here the creep /relaxation, and the data acquisition have impact on the measurement result.

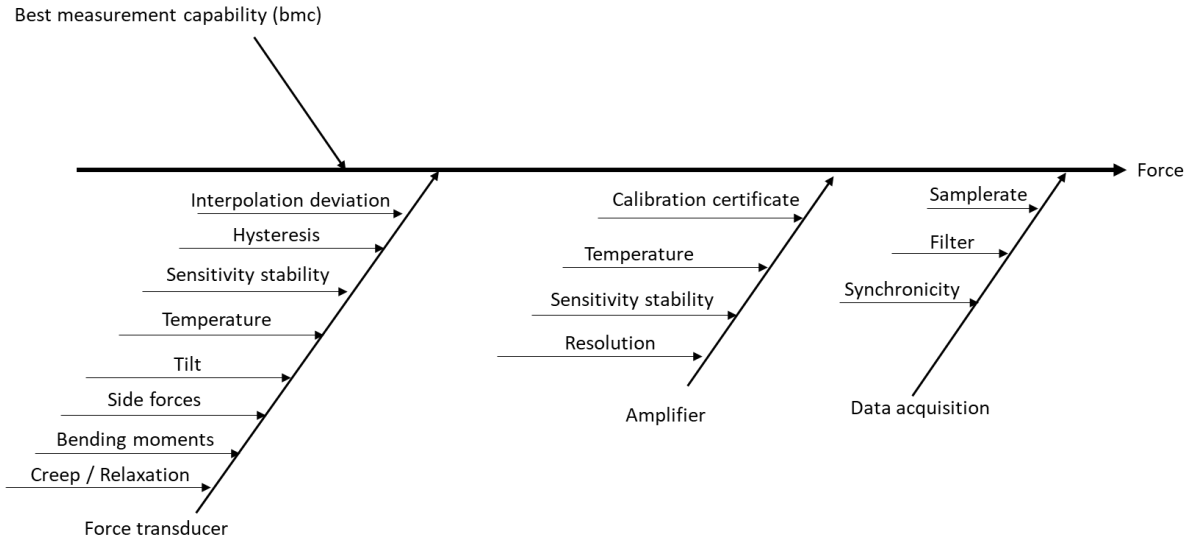

Figure 27 Ishikawa diagram of the influences on a continuous force measurement

DOI 10.5281/zenodo.7113187

3.2 Creep / Relaxation:

The observed “creep” effect of force transducers is the result of many force-time dependent effects within the spring material, the strain gauge, and the bonding between those two elements. It is mainly the overlay of three different effects:

- Viscoelastic behaviour of the foil of the strain gauge and the glue between strain gauge and spring material. The stretched measuring grid acts like a stretched spring. The spring force generates shear stresses at the contact surfaces between the measuring grid and the carrier, in addition to the normal stresses resulting from the expansion. Under the influence of these stresses, the plastics of the strain gauge and the adhesive relax, i.e. the opposing force subsides and the measuring grid retracts.
- Thermoelastic effect of the spring element. Due to a certain tension, the material cools down and due to a certain compression the material heats up. If one waits for the temperature to equalize between the stretched and compressed areas, additional compression or expansion of the corresponding areas goes hand in hand with the cooling of the compressed and the warming of the stretched areas.
- Material creep of the spring element, which are atomic place changing processes.

[12], [13], [3], [14]

All these effects cannot be modelled separately that is why they are summarized and described rheologically by a series of Kelvin-Voigt Elements.

In order to describe the short-term creep of the force transducer, it has been proven practically to use up to three Kelvin-Voigt Elements in series (equation 11)

$$\delta = (1 - d(F)) \cdot \frac{F}{k_0} + F\left[\left(\frac{1}{k_1} - \frac{1}{k_1} e^{-\frac{k_1}{D_1}t}\right) + \left(\frac{1}{k_2} - \frac{1}{k_2} e^{-\frac{k_2}{D_2}t}\right) + \left(\frac{1}{k_3} - \frac{1}{k_3} e^{-\frac{k_3}{D_3}t}\right)\right] \tag{11}$$

Investigation:

The same transducers as for the validation for the sensitivity were used with the same amplifiers with the same settings as for the validation of the instantaneous sensitivity.

The transducers were loaded with the maximum capacity of the transducer in the fastest amount of time possible by the deadweight machine. The load then was kept constant for 300 seconds until it was unloaded completely as fast as possible. For the Dynamometer this was also repeated in force steps ranging from 10 % to 100 % nominal load.

Evaluation:

For a better comparison between the transducers, the creep behaviour was normalized to the value 30 seconds after the application of the maximum load. The resulting curves were then fitted using the least square method. This was done with the solver function using the gradient method within the excel software. For the evaluation of the measurement results of the Dynamometer the Origin software, which uses for the fitting the Levenberg Marquardt method, was used.

Results:

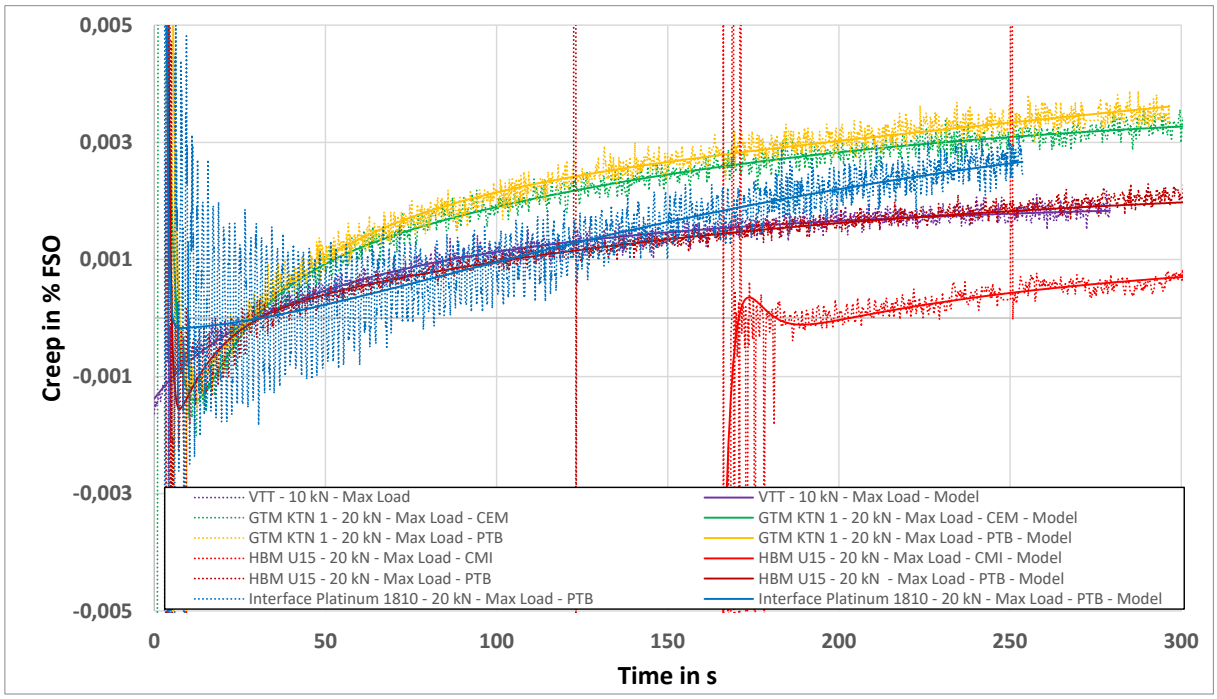

Figure 28 Short-term creep behaviour of class 00 force transducers with positive creep

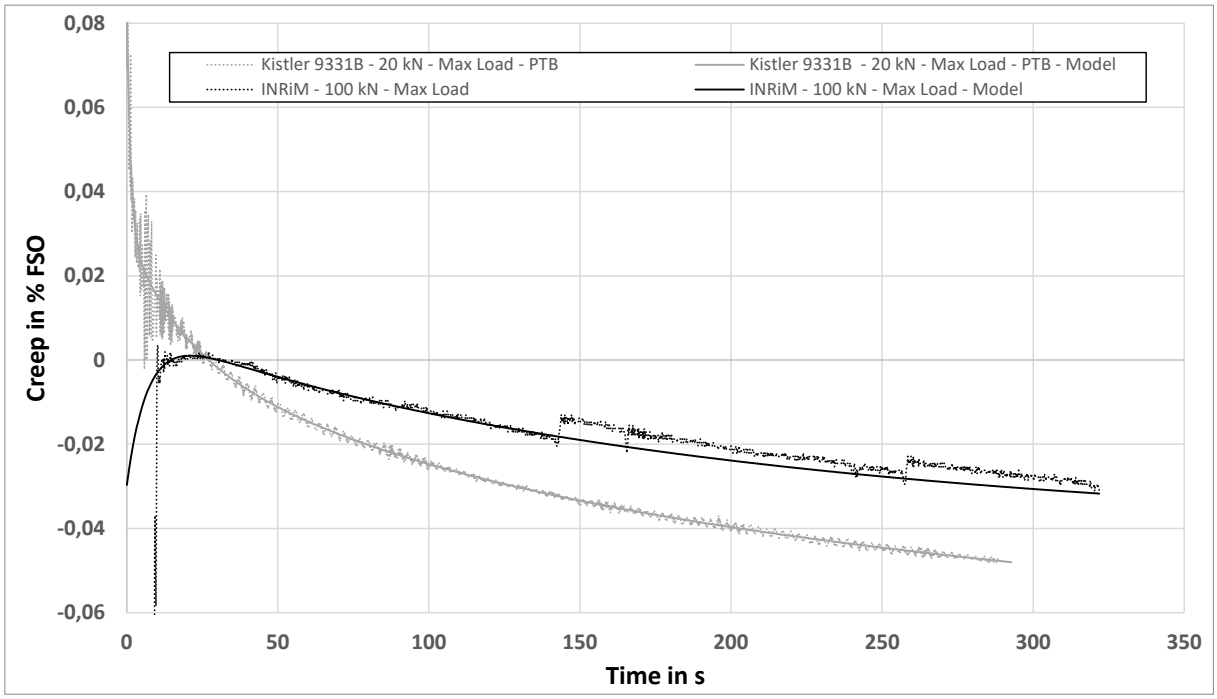

Figure 29 Short-term creep behaviour of a class 0.5 strain gauge and piezoelectric force transducer with negative creep

DOI 10.5281/zenodo.7113187

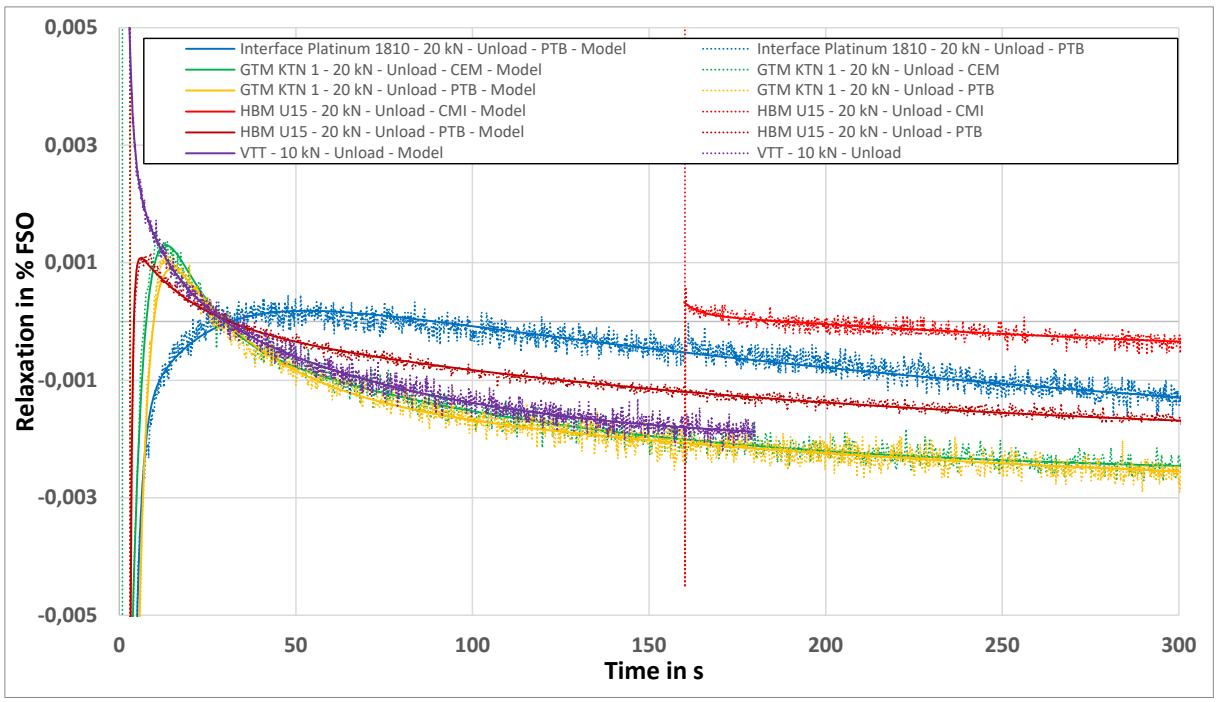

Figure 30 Short-term relaxation (or unloading creep) of class 00 force transducers

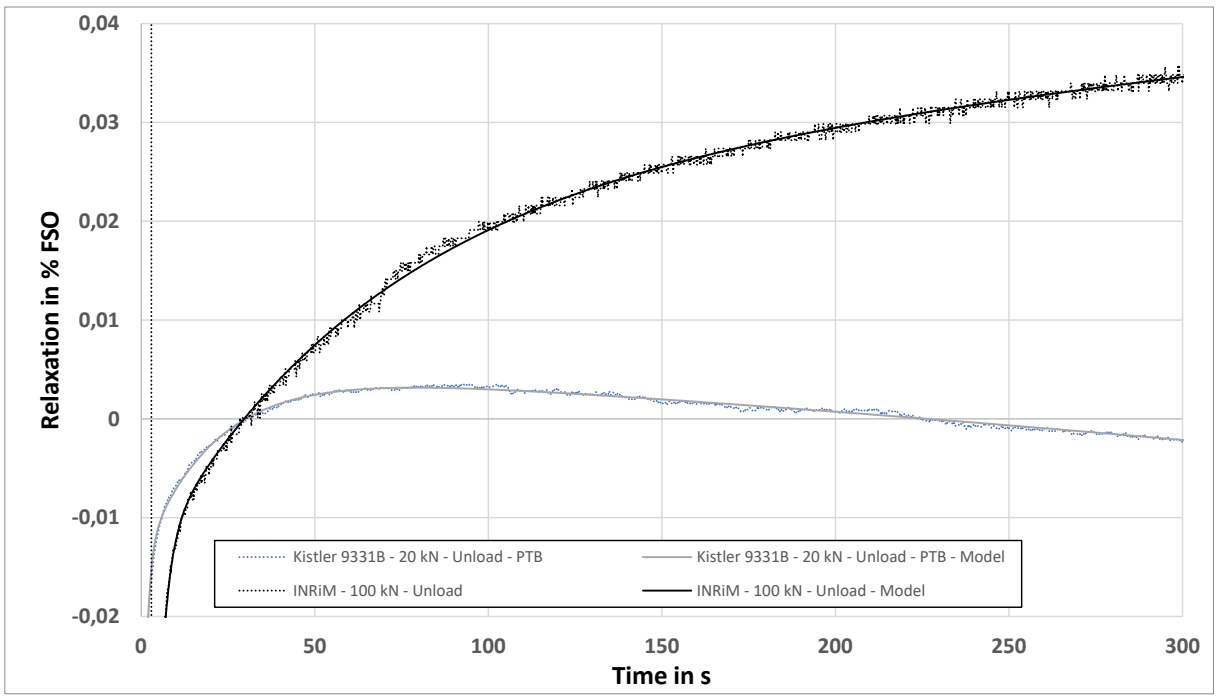

Figure 31 Short-term relaxation (or unloading creep) of a class 0.5 strain gauge and piezoelectric force transducer

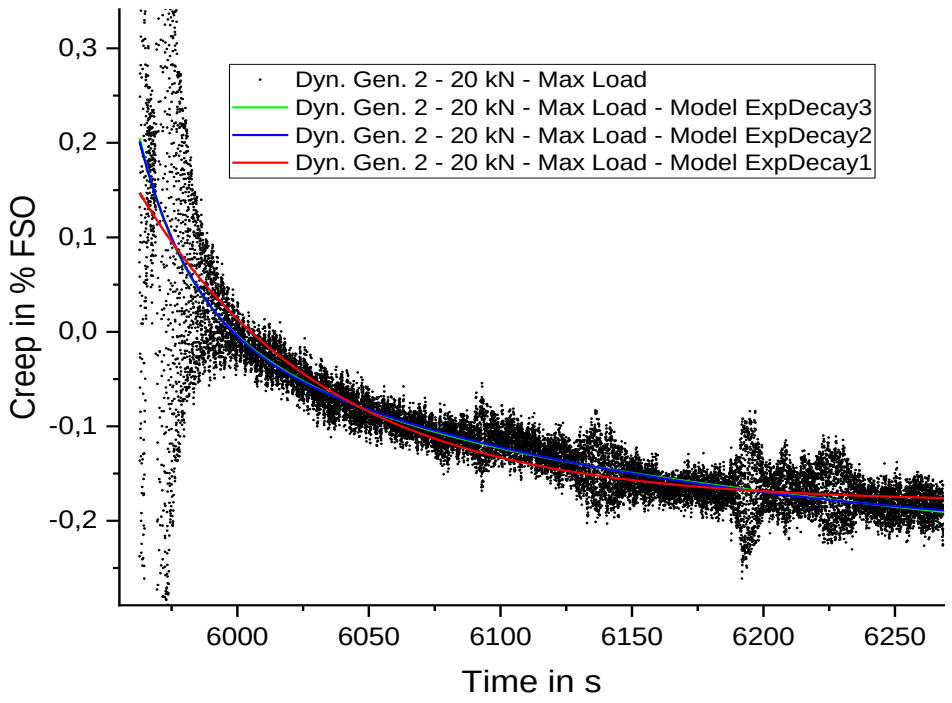

Figure 32 Short-term creep of the Dynamometer 2. Generation Stutt (no classification) with strong negative creep

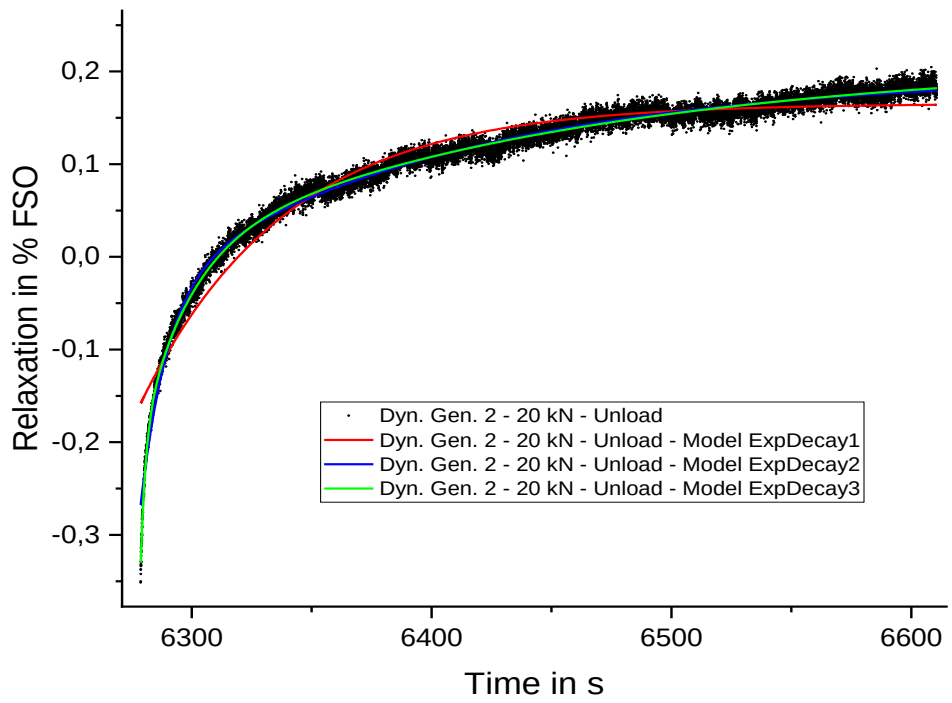

Figure 33 Short-term relaxation (or unloading creep) of the Dynamometer 2. Generation Stutt (no classification)

DOI 10.5281/zenodo.7113187

Table 2 Model parameters to the relaxation behaviour of the Dynamometer 2. Generation Stutt

Model	ExpDecay1
Equation	y = y0 + A1*exp(-(x-x0)/t1)
Plot	I
y0	0,16543 ± 2,10992E-4
x0	6264,44033 ± --
A1	-0,40977 ± --
t1	60,57876 ± 0,20917
Reduced Chi-Sqr	3,03023E-4
R-Square (COD)	0,95263
Adj. R-Square	0,95262

Model	ExpDecay2
Equation	y = y0 + A1*exp(-(x-x0)/t1) + A2*exp(-(x-x0)/t2)
Plot	I
y0	0,19653 ± 3,53667E-4
x0	6276,56356 ± 97188,38358
A1	-0,28538 ± 2466,81829
t1	11,24364 ± 0,06952
A2	-0,23383 ± 177,71256
t2	127,87659 ± 0,7197
Reduced Chi-Sqr	6,5673E-5
R-Square (COD)	0,98973
Adj. R-Square	0,98973

Model	ExpDecay3
Equation	y = y0 + A1*exp(-(x-x0)/t1) + A2*exp(-(x-x0)/t2) + A3*exp(-(x-x0)/t3)
Plot	I
y0	0,21237 ± 7,51342E-4
x0	6278,1296 ± --
A1	-0,18163 ± --
t1	2,04715 ± 0,04503
A2	-0,20496 ± --
t2	19,40112 ± 0,20805
A3	-0,21213 ± --
t3	171,18259 ± 1,92584
Reduced Chi-Sqr	5,132E-5
R-Square (COD)	0,99198
Adj. R-Square	0,99198

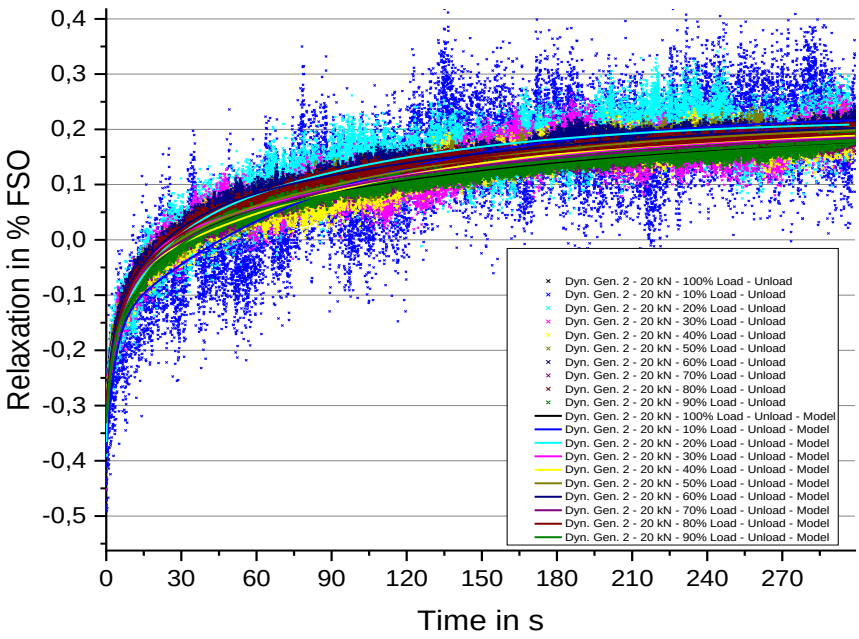

Figure 34 Short-term relaxation behaviour of the Dynamometer 2. Generation Stutt from different load levels in the range of 10 to 100 % of the transducers capacity

Conclusion:

All short-term creep and unloading creep behaviours of the investigated force transducers could be sufficiently described by a series of up to three Kelvin-Voigt cells. A further investigation of the Dynamometer showed that the observed behaviour could be linear scaled to every force level in the range from 10 to 100 % FSO. Even though the time dependent effects of a piezoelectric force transducer differ from a strain gauge transducer, its behaviour could also be described with a model consisting out of three Kelvin-Voigt cells. But in addition to this the linear drift behaviour of the charge amplifier needs to be added here.
[15], [16], [5], [17], [18]

3.3 Temperature:

Additionally to the sensitivity and the zero point the creep / relaxation behaviour of a force transducer is influenced by temperature.
[18], [3], [14]

Investigation

For this investigation the GTM KTN 1 with 20 kN capacity was measured twice on the 200 kN FSM with temperature chamber at PTB. The first time with the DMP 40 as amplifier and one year later with the Dewetron DAQP STG as amplifier.

The creep and unloading creep behaviour was investigated in 5 °C steps in a range of 10 to 30 °C. The transducer was after stabilization of each temperature loaded to its maximum capacity (20 kN) and its creep behaviour was measured. After this the transducer was completely unloaded again and its unloading creep behaviour was measured. The machine needed 21 seconds until the load was fully applied or released.

DMP 40	Dewetron DAQP STG
Measuring principle: Carrier-frequency (225 Hz) Filter settings: 0.1 Hz to 1.7 Hz Samplerate: 0.1 Hz to 5 Hz Creep /Unloading creep duration: 20 minutes	Measuring principle: DC Filter settings: 300 kHz Samplerate: 1000 Hz Creep /Unloading creep duration: 10 minutes

Results

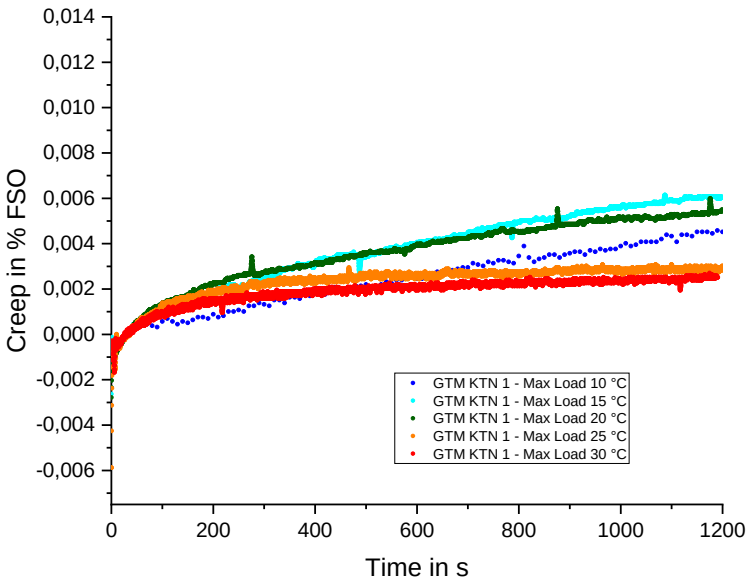

Figure 35 Creep behaviour of the GTM KTN 1 with DMP 40 at different temperatures in a range from 10 to 30 °C

DOI 10.5281/zenodo.7113187

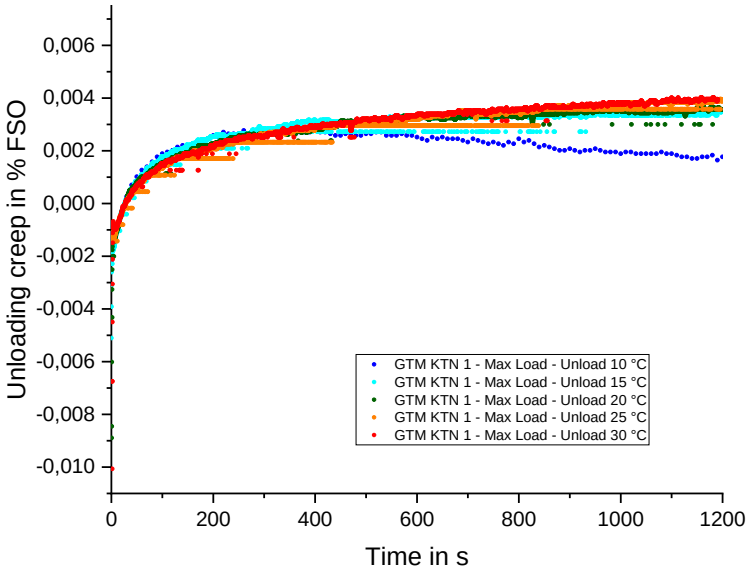

Figure 36 Unloading creep (relaxation) of the GTM KTN 1 with DMP 40 at different temperatures in a range from 10 to 30 °C (results were multiplied with -1)

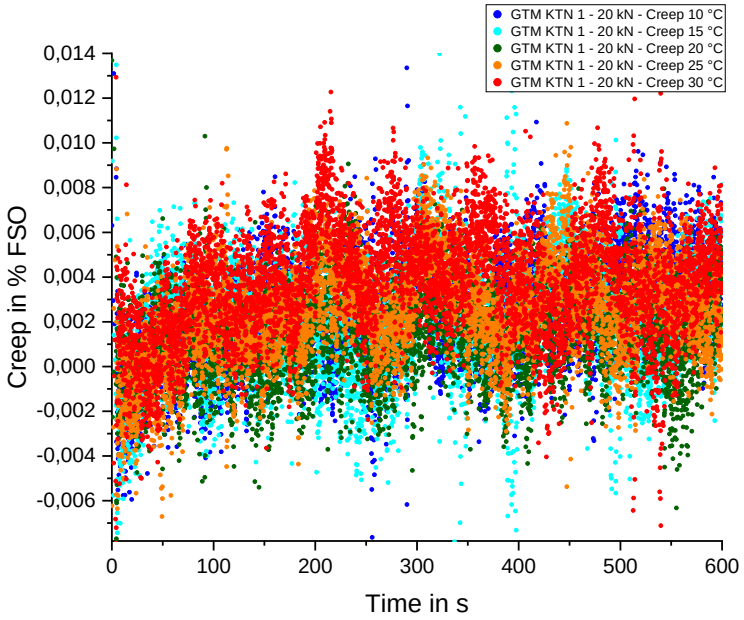

Figure 37 Creep behaviour of the GTM KTN 1 with Dewetron DAQP STG at different temperatures in a range from 10 to 30 °C

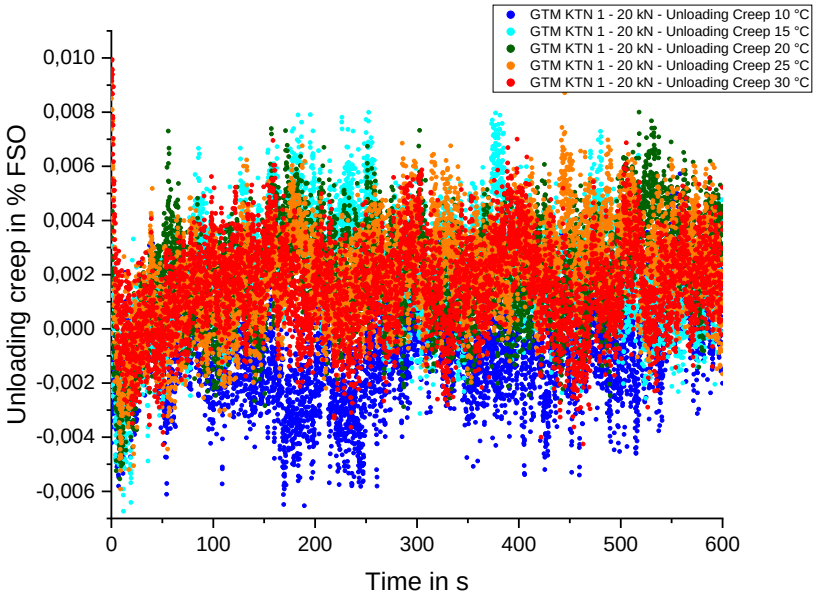

Figure 38 Unloading creep (relaxation) behaviour of the GTM KTN 1 with Dewetron DAQP STG at different temperatures in a range from 10 to 30 °C (results were multiplied with -1)

Conclusion:

For the measurements with the Dewetron DAQP STG only the unloading creep at 10 °C differed significantly. For the measurements with the DMP 40 for the loading creep a slight trend could be observed. Here the creep behaviour subsided earlier with increasing temperature.

3.4 Amplifier and data acquisition:

The force measuring chain consists of the force transducer, the amplifier and an indicator or data acquisition software. For static measurements, the amplifier is calibrated with regard to its static transfer behaviour as a function of the amplitude. For continuous force measurements, however, the influence of the filter settings, synchronicity of the channels, the signal to noise ratio and the sampling rate of the data acquisition must also be taken into account.

In all previous investigations within this report, mainly two different types of amplifiers were used. On the one hand a carrier frequency amplifier (DMP 40 / 41 from HBM) and on the other hand a DC amplifier (Dewetron DAQP STG). The main benefit of the carrier frequency amplifier are its high resolution with very low signal to noise ratio (as it can be seen in Figure 35 and Figure 36), which is why it is particularly well suited for static measurements. However, a limiting factor here is the low sampling rate and the low filters that cannot be switched off. A filter setting of 1.7 Hz Bessel with a sampling rate of 5 Hz has proven to be a good compromise for this amplifier for continuous measurements. The influence of the 1.7 Hz Bessel filter on a step response was tested using the brigde standard K3608 (see Figure 38)

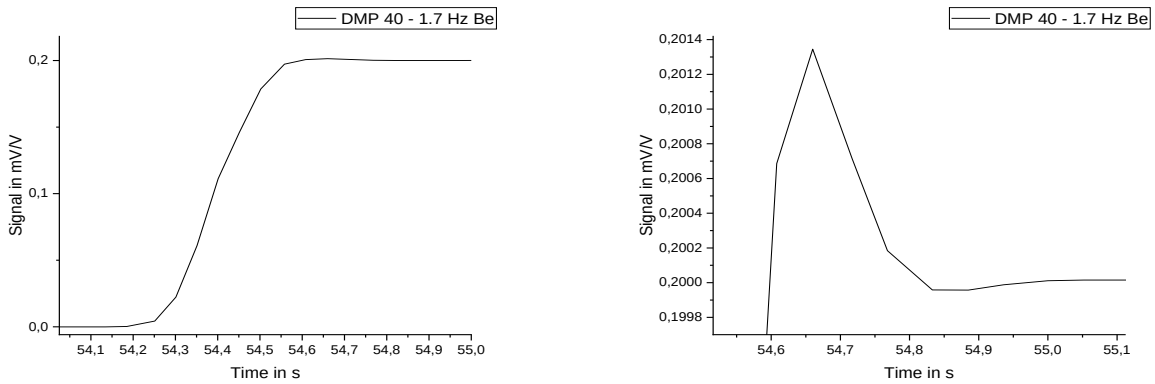

Figure 39 Delay and overshoot behaviour of the DMP 40 1.7 Hz Bessel filter setting when a step function is applied to the system

DOI 10.5281/zenodo.7113187

The main benefits of the DC amplifier are its high sampling rate, linear phase behaviour and high low-pass filter, which is why it is particularly well suited for dynamic measurements. However, a limiting factor here is the signal to noise ratio (see Figure 37 and Figure 38), which here had a maximum of 0.008 % at full scale output. With a target uncertainty of 0.1 % for continuous force measurements, the advantages of the DC amplifier outweigh this, since in addition to the unadulterated signal, the error in synchronization of data streams also becomes smaller with higher sampling rate.

The transfer function of the used amplifier has to be considered regarding the signal which passes the amplifier. The common approach is the application of the Nyquist plot by a fourier transform of the measured time signal, compensating of the amplifier transfer function and an inverse fourier transform.

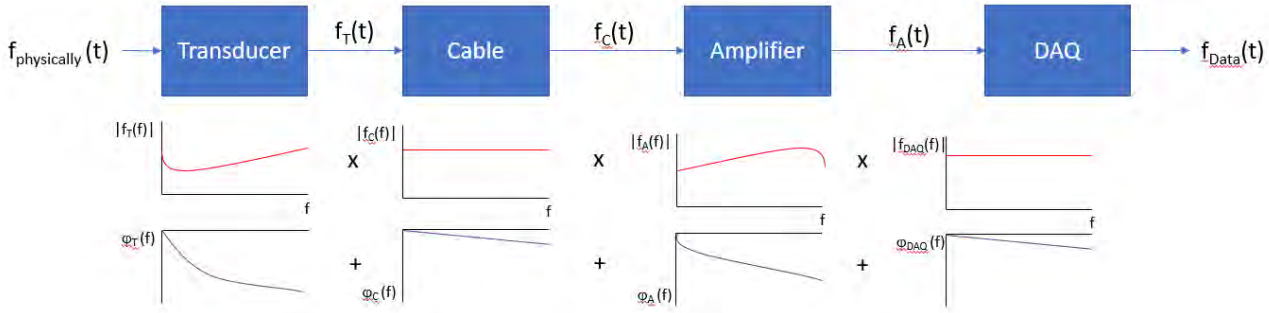

Beside disadvantages as e.g. likely leakage effects this high effort approach is might often skipped in practice by just dividing the time signal by ABS values of the transfer function. But this is only meaningful in a very narrow area of several boundary conditions.

The consideration of the amplifier as dispersion system was proven as an effective additional approach to describe the changes of a passing time signal. This approach is also very useful for the assessment and understanding of the necessary compensation. Let`s assess the following example of a time signal. The signal is not a harmonic with a constant amplitude but a signal with an envelope and a harmonic part. The term "group velocity" describes the velocity of the envelope (red) and the "phase velocity" describes the velocity of the harmonic part (blue).

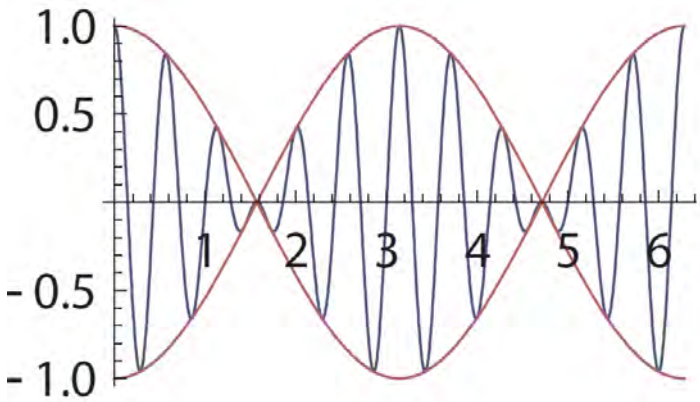

$$v_P = -\frac{\varphi_{Amplifier}(f)}{f}$$

$$v_G = -\frac{d\varphi_{Amplifier}(f)}{df}$$

These different time parameters have only the same value as long as the phase is perfect linear. If so the signal, no matter what form it has, will pass the amplifier by constant value of time. If not, so the signal will be distorted even if the ABS transfer function is constant.

The behavior of the amplifier can be separated into the transfer function of the amplifier itself and the influence of the applied filter. Some amplifiers offer the opportunity to shut all filters of. This would leave the transfer function of the absolute value by the bandwidth of the amplifier itself as shown in the next figure. The common Bessel filter of different orders and different cutoff frequencies influences not only the ABS but also the phase.

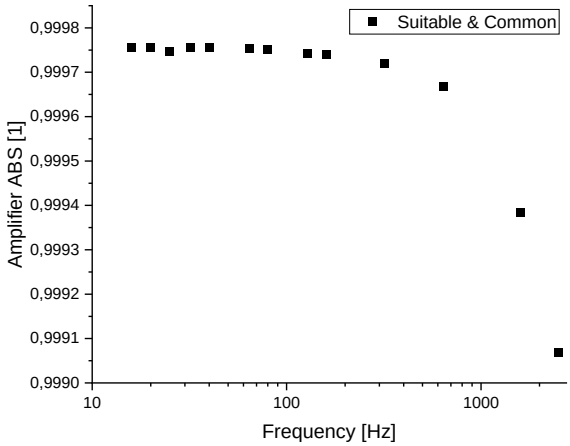

A common practice at this point might be to set the cutoff frequency just as high as possible to avoid such distortions. But without evaluation no one can be sure that this really works as supposed. The following figure shows a comparison of two different amplifiers. The amplifier with the unsuitable phase was an amplifier with a maximum cutoff frequency of 100 kHz. This value seems to be pretty high and it is meaningful to see it that way as long as we only consider the transfer function of the absolute value. But here we can see that the phase is distorted in strong nonlinear way. The frequency band of this distortion is in particular important for continues and low frequency measurements in material testing machines. To set the cutoff frequency as high as possible can work regarding a linear phase but it does not have to.

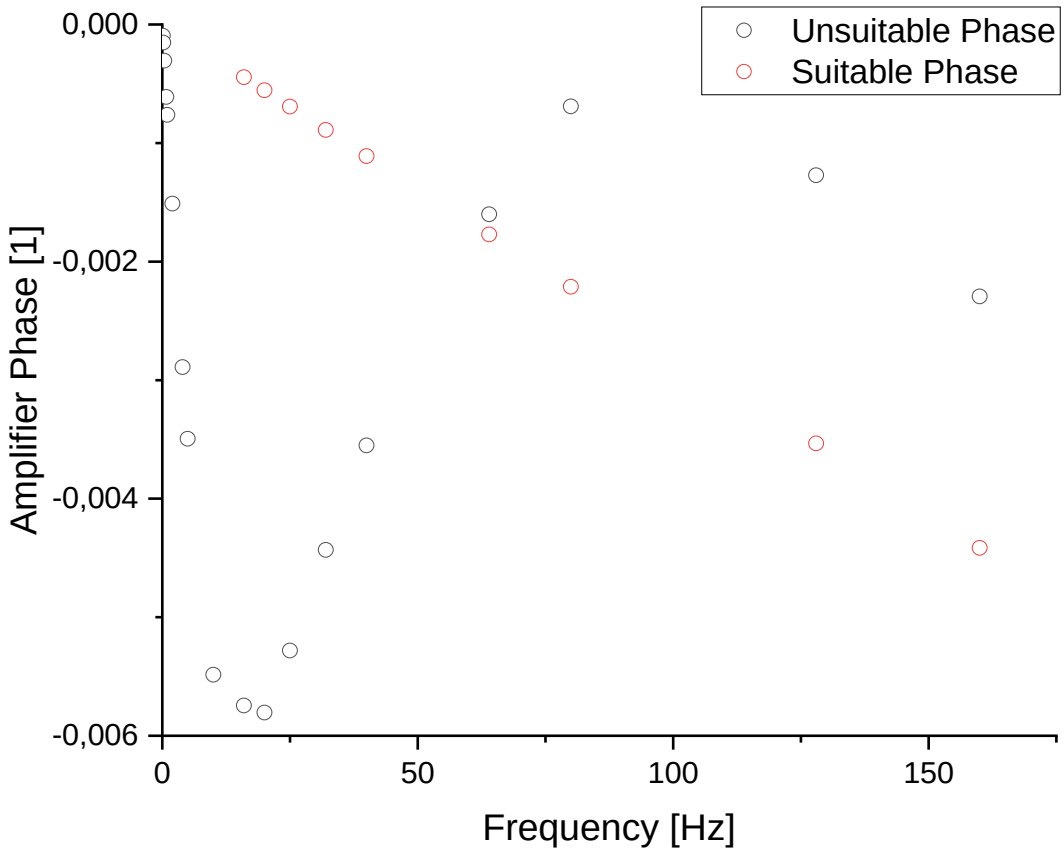

[19]

DOI 10.5281/zenodo.7113187

4 Validation limits:

The investigations carried out for this report also revealed limitations within which the model presented here could be validated.

Within this report, the hysteresis that influences the sensitivity to decreasing forces was not examined in detail. Investigations and possible models (Maxwell-Slip and Preisach-Krasnoselski) for this were mentioned in [20] and [3]. These are numerical models that require a large number of parameters which have to be determined in a complex manner. In addition, the hysteresis is influenced by the creep behaviour. [17], [21]

The creep behaviour was examined here for a maximum of 20 minutes, which is why statements about force-time profiles are not validated over a longer period of time. A limiting factor was also the load change time of the deadweight machine and the filter setting used for the amplifier. This totaled up to 3.5 seconds, which could be reduced with a higher uncertainty to 2.3 seconds by using a DC amplifier. So statements for continuous forces faster than 2.3 seconds from zero to the specific force in a range between 10 to 100 % of the transducers capacity are not validated.

The creep analyses were done on a FSM with hard compression plates and stiff construction of the reference station. When using a more compliance base this might influence especially the short-term creep behaviour. [22]

The tilting analysis was restricted to the compression mode.

The influence of temperature was examined here from 10 to 30 °C, which is why statements outside of this range cannot be made. Furthermore, these were temperatures in equilibrium, which is why these statements on the temperature-dependent behaviour of force transducers that are exposed to a temperature gradient are not applicable.

5 Practical model:

The sensitivity of force transducers for static and continuous forces is given by the instantaneous elongation of the spring element after a load step. This can be described with a third-degree polynomial

$$F_{Tra} = R' \cdot X_{instant}^3 + S' \cdot X_{instant}^2 + T' \cdot X_{instant} \tag{12}$$

in which F_{Tra} is the force which is applied on the transducer, $X_{instant}$ the instantly indicated signal of the force transducer in its calibration and R', S' and T' are its sensitivity coefficients.

To incorporate the in this report discussed influences a product model with correction factors is proposed

$$F = F_{Tra} \cdot \prod_{i=1}^{10} K_i \tag{13}$$

$$\prod_{i=1}^{10} K_i = K_{bmc} \cdot K_{amp} \cdot K_{creep} \cdot K_{T_{Sens}} \cdot K_{Stab} \cdot K_{T_{Zero}} \cdot K_{tilt} \cdot K_{side} \cdot K_{bend.mom.} \cdot K_{DAQ} \cdot K_{T_{creep}} \tag{14}$$

$$K_i = \left(1 + \frac{\delta x_i}{|x_i|}\right) \tag{15}$$

There are two possible ways. First, the error δx_i is significant and can be modelled and should therefore incorporated as a correction factor with an uncertainty of the correction. Second, the error cannot be modelled or is insignificant, then the error is set to 0 and an uncertainty estimation has to be made, which is to be incorporated into the measurement uncertainty budget.

DOI 10.5281/zenodo.7113187

With

bmc	Best measurement capability
K	Correction factor
creep	creep
T_{Sens}	Temperature on sensitivity
T_{Zero}	Temperature on zero
T_{Creep}	Temperature on creep
amp	amplifier
tilt	Tilted reference force
side	Side forces
bend. mom.	Bending moments (including misalignments)
DAQ	Data acquisition

References

[1] R. A. Mitchell and S. M. Baker, „Characterising the creep response of load cells," *VDI-Berichte Nr 312,* pp. 43-48, 1978.

[2] L. Nasdala, FEM - Formelsammlung Statik und Dynamik, Wiesbaden: Vieweg+ Teubner | Springer Fachmedien, 2012.

[3] H. Kortendieck, „Development and testing of models for creep and hysteresis correction," VDI-Verlag, Düsseldorf, 1993.

[4] „ISO 376:2011, Metallic materials - Calibration of force-proving instruments used for the verification of uniaxial testing machines".

[5] J. Sander, „Comparison of force measuring devices with static and continuous loading," in *XXIII IMEKO World Congress*, Yokohama, Japan, 2021.

[6] A. Nitschke, S. Neumann, S. Gerber, R. Kumme and F. Tegtmeier, „Development of a force transfer standard for the calibration of cyclical forces in materials testing machines with quantification of parasitic factors," in *Proc. of Sensoren und Messsysteme*, Nuremberg, 2022.

[7] EURAMET e.V. cg-4, „Uncertainty of force measurements," 2011.

[8] D. Röske, „Linear regression analysis and the GUM: Example of temperature influence on force transfer transducers," in *IMEKO 24th TC3 International Conference*, Cavtat-Dubrovnik, Croatia, 2020.

[9] A. Prato, S. Palumbo, A. Germak, F. Mazzoleni and P. Averlant, „Effects due to the misalignment of build-up systems for force measurements in the meganewton range," *Journal of Physics: Conference Series, Vol. 1065, No. 4,* 2018.

[10] A. Prato, E. Giacardi, A. Facello, F. Mazzoleni and A. Germak, „Influence of parasitic components in the static calibration of uniaxial force transducers," in *IMEKO 24th TC3 International Conference*, Cavtat-Dubrovnik, Croatia, 2022.

[11] „DKD-R 3-9: 2018, Continuous calibration of force transducers according to the comparison method".

[12] K. Hoffmann, „Zur Herstellung moderner Folien-Dehnungsmessstreifen und den dabei gegebenen Korrekturmöglichkeiten für Kriechen und Querempfindlichkeit," *Messtechnische Briefe 22 Heft 2,* pp. 41-47, 1986.

[13] S. Keil, Dehnungsmessstreifen, Wiedbaden: Springer Vieweg, 2017.

[14] M. Kühnel, „Traceable measurement of the mechanical properties of spring elements for the force measurement technology," Phd. thesis at the University of Ilmenau, 2013.

[15] O. Mack, „Behaviour of piezoelectric force transducers under the impact of mechanical influence quantities,“ PTB-MA-77, Braunschweig.

[16] J. Tichý and G. Gautschi, Piezoelectric Measuring Systems, Berlin Heidelberg New York: Springer, 1980.

[17] J. Sander, „Creep correction method for force applications,“ in *IMEKO 24th TC3 International Conference*, Cavtat-Dubrovnik, Croatia, 2022.

[18] T. W. Bartel and S. L. Yaniv, „Creep and creep recovery response of load cells tested according to U.S. and international evaluation procedures,“ *Journal of Research of the National Institute of Standards and Technology Volume 102 Number 3,* 1997.

[19] L. Klaus, M. F. Beug and T. Bruns, „A new calibration set-up for the dynamic calibration of brigde amplifiers from DC to 10 kHz,“ in *IMEKO 23rd TC3, 13th TC5 and 4th TC22 International Conference*, Helsinki Finland, 2017.

[20] T. Rabault, P. Averlant and F. Boineau, „Numerical modelling of hysteresis applied on force transducer,“ in *XXI IMEKO World Congress " Measurement in research and Industry*", Prague, Czech Republic, 2015.

[21] G. Haucke, R. Kumme and E. H. Hasan, „Effect of different loading schemes on creep and creep recovery for force measurements,“ in *IMEKO 2010 TC3 Conferences Metrology in Modern Context*, Chonburi, Thailand, 2010.

[22] J. D. Fidelus and K. Cybul, „Study on short-term creep effect and hysteresis for the HBM Z4A force transducer under compressive and tensile forces,“ *Acata IMEKO9 (2020) 5,* pp. 137 - 142, 2020.

DOI 10.5281/zenodo.7113187

10.5281/zenodo.7113187

Part B
Dynamic forces

EN

Dynamic

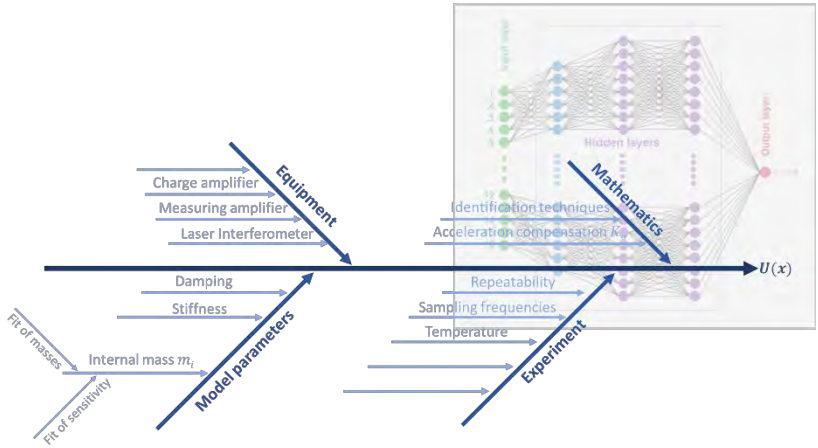

DOI: 10.5281/zenodo.7113187

Part B
Dynamic forces

Version 1.0

Editors

Physikalisch Technische Bundesanstalt, Germany:
D. Mirian, F. Hauschild, S. Hassan, R. Kumme

RISE, Sweden:
M. Wozniak

Comprising the results from our research and the fruitful and intensive discussions with all our other project partners worldwide.

Contact: comtraforce@ptb.de

Braunschweig September 2022

Table of Contents

Introduction: 48

Dynamic force calibration setup: 48

Mathematical model (Advanced Kelvin-Voigt model): . 50

Correction factor for the top mass: 51

Static sensitivity: 52

Measurement procedure: 55

Evaluation: 57

Measurement results: 58

Internal mass *58*

Dynamic sensitivity of force transducer *61*

System Identification: 63

Frequency Domain *64*

Stiffness: 64

Damping: 65

Time Domain *65*

ARMAX and BJ Models 66

Deep Learning Models 66

Temperature effects 72

Conclusion 73

Uncertainty analysis of the parametric identification: . 74

Parameters *74*

Internal mass 75

Dynamic sensitivity 75

Stiffness 76

Damping 76

Deep neural networks DNN 76

References 78

DOI 10.5281/zenodo.7113187

Introduction:

Despite the well-established procedure for static calibration of force transducers described in ISO 376 [1], the dynamic calibration of the sensor has been always challenging because of some reasons such as the sophisticated nature of dynamic measurement, insufficient structural equipment, and parasitic effects which yield higher measurement uncertainty in comparison to static measurements and therefore inappropriate characterization of the force transducers. However, there are some efforts to model transducers under dynamic force conditions [2, 3, 4].

Dynamic force calibration setup:

The force transducer is mounted via a mechanical adapter (plate) on the top of an electrodynamic shaker which is able to generate sinusoidal forces at different frequencies from low frequencies up to more than 2 kHz and also periodic chirp signal which sweeps over a wide spectrum of frequency. This in turn enables rapid investigation of the frequency response of the system (see Figure 40).

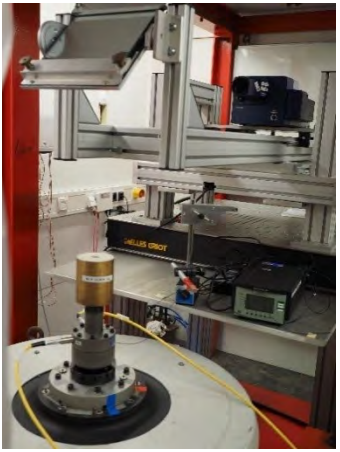

Figure 40 PTB dynamic force calibration setup

The force transducer is equipped with several cylindrical masses during the measurements. The acceleration is measured by a scanning laser interferometer which is able to carry out point-by-point acceleration measurements on a lattice of the desired shape.

An alternative method of measuring acceleration is using acceleration sensors instead of an interferometer. In this case, the acceleration of the cylindrical load mass and the acceleration of the base mass on the mounting plate of the shaker should be recorded (note: the analysis of the transverse movements of the shaker's moving part and the loading mass can be performed by using e.g. 3-axial accelerometers). Figure 2 shows the schematic layout of the measurement system. This method, verified in RISE, is dedicated for accredited laboratories and for industrial applications.

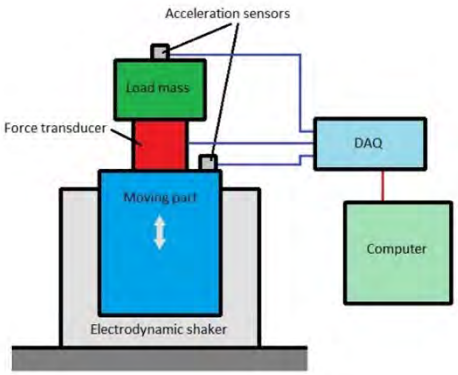

Figure 41 Schematic of calibration setup with alternative acceleration measurement

DOI 10.5281/zenodo.7113187

Mathematical model (Advanced Kelvin-Voigt model):

A force transducer under dynamic force conditions can be modeled as a head mass which is connected to its base mass by a spring of constant k_f, and a damper with a damping coefficient b_f. The load mass is mounted on the force transducer (see Figure 42).

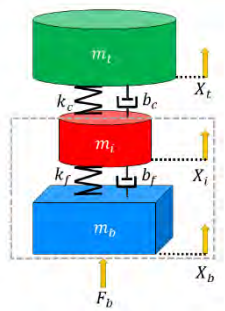

Figure 42 Kelvin-Voigt model for the force transducer and the mounted top mass other dynamic conditions

The dynamic sensitivity S_f of the force transducer, given in equation (1), is the result of periodic calibration. It represents the ratio between the output signal from the transducer U_f and the generated dynamic force F. This force is the product of mass and acceleration. The acceleration is measured on the top of the load mass giving $a_{\mathrm{t}}(f)$. Whereas the mass responsible for the dynamic force sensed by the transducer is composed of the internal mass m_i,the mass of stiff adaptation elements m_{a} and the top mass m_t that is corrected by the factor K_0 representing its non-rigidity.

$$S_f = \frac{U_f}{a_t(f).[(m_a + m_i) + (m_t.k_0)]} \qquad (1)$$

The internal mass m_i of the force transducer is defined as a part of the calibration procedure. The product of the top mass m_t and a correction factor described in the next section is taken to account.

Correction factor for the top mass:

Since the top mass cannot be seen as a rigid body, an appropriate correction factor K_0 should be calculated for each mass. Thereby the vibrational modes of each mass point are considered. In equation (2), l is the vertical dimension of the top mass and ω angular frequency.

$$K_0 = \frac{\sin(\sqrt{k_m \omega^2} l)}{\sqrt{k_m \omega^2} l} \qquad (2)$$

The material-specific k_m is defined as the ratio between ρ density and E Young's modulus:

$$k_m = \frac{\rho}{E} \qquad (3)$$

As the measurements are performed with masses of the same material, k_m is same for all measurements. Figure 43 demonstrates the frequency-dependent correction factor for 1 kg to 4 kg cylindrical top brass masses used for the force transducer calibration.

DOI 10.5281/zenodo.7113187

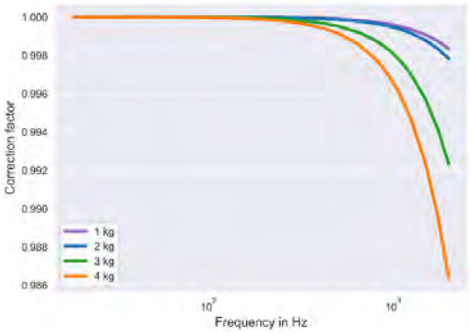

Figure 43 correction factor for the different cylindrical brass mass

Static sensitivity:

The sensitivity of the force transducer under dynamic conditions as a function of frequency S_f is compared to the static sensitivity S_{f0} extracted from the calibration certificate as the main part of the dynamic force investigation. Linear regression yields the line of best fit to measurement data in both compression and tension modes. The average slope of these two lines is taken as the static sensitivity.

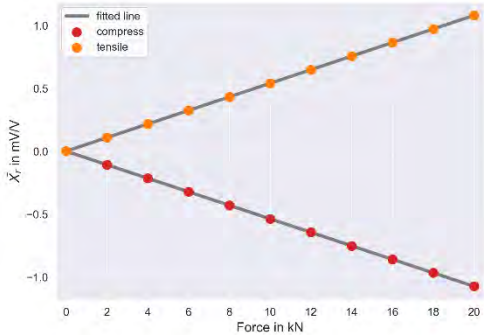

Figure 44 static force measurements performed on the transducer developed by MPA Stuttgart and corresponding linear regression

Figure 44 demonstrates static force measurement results in the compress and tensile directions for the stain gauge force transducers developed by the MPA university Stuttgart in cooperation with the PTB and HBK introduced in part A of this report. Measurement and evaluation results of this transducer are chosen for the whole parts in this report. Figure 45 demonstrates the above-mentioned force transducer on the electrodynamic shaker.

DOI 10.5281/zenodo.7113187

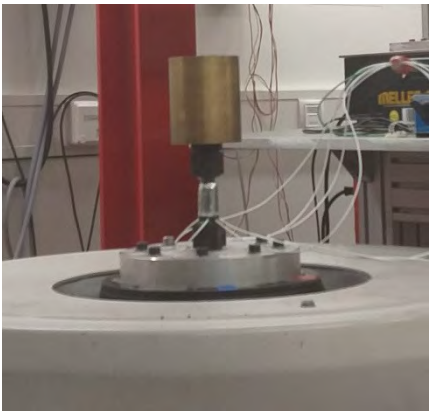

Figure 45 self-manufactured strain gauge on the electrodynamic shaker

Moreover, the following three force transducers were selected at RISE for dynamic calibration.

Piezoelectric (ICP) force transducer: **Type:** 208C05 **Manufacturer:** PCB **Nominal range:** 22.24 kN (C) / 2.224 kN (T) **Static sens.** S_{f0} 0.2187 mV/N	Strain gauge transducer: **Type:** U10M **Manufacturer:** HBM **Nominal range:** 5 kN **Static sens.** S_{f0} $2{,}476 \cdot 10^{-4}$ (mV/V)/N	Strain gauge transducer: **Type:** U10M **Manufacturer:** HBM **Nominal range:** 50 kN **Static sens.** S_{f0} $4{,}116 \cdot 10^{-5}$ (mV/V)/N

HBM QuantumX MX410B was used as DAQ for these transducers as well as for acceleration sensors (PCB, type ICP). This system allows synchronized measurement data acquisition, with sampling rate up to 100 kS per individual channel. RISE has chosen not to use any filters for their measurements.

Measurement procedure:

The electrodynamic shaker is excited to generate sinusoidal displacement with desired amplitude. By carefully selecting the excitation voltage for each setup with the different mass, the acceleration on top mass and hence force at each frequency can be kept constant. As for the acceleration equal to 50 $\frac{m}{s^2}$ the measurement results reveal the best results on the PTB dynamic force calibration system, this value is selected as the optimum acceleration to perform comparable measurements. However, a minimum excitation voltage limit to 10 mV in the controlling system restricts the constant acceleration generation over all frequencies, especially close to the system resonance frequency where the excitation voltage must be reduced below 10 mV. Figure 46 represents the amplitude of the excitation voltage needed to generate constant acceleration on the top mass.

DOI 10.5281/zenodo.7113187

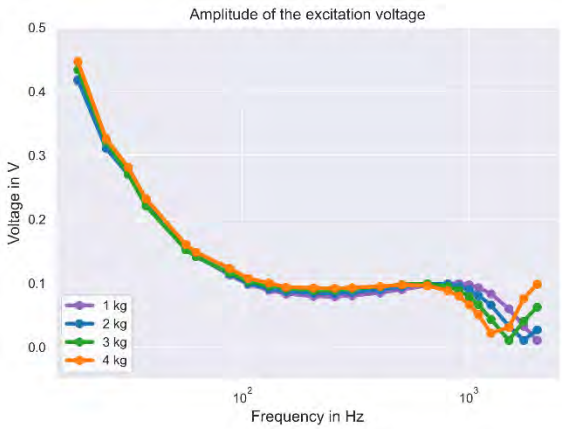

Figure 46 excitation voltage applied to the shaker to generate 50 $\frac{m}{s^2}$ acceleration on the top mass

Table 3 is the numeric demonstration of the same measurement as mentioned in Figure 46. The values shown in red represent the actual excitation voltage put during measurements in the controlling system.

	Excitation Frequency in Hz	No. of Sample	Excitation Voltage in Volt			
			1 kg	**2 kg**	**3 kg**	**4 kg**
1	18.75	8192	0.4162	0.4178	0.4335	0.4464
2	25	8192	0.3221	0.3105	0.3209	0.3258
3	31.25	8192	0.2794	0.2699	0.2707	0.281
4	37.5	4096	0.2274	0.2263	0.2204	0.2316
5	56.25	4096	0.1544	0.1552	0.1519	0.16
6	62.5	4096	0.1421	0.1413	0.1411	0.1479
7	87.5	4096	0.1127	0.114	0.1158	0.1229
8	106.25	4096	0.0978	0.0993	0.1025	0.1072
9	131.25	4096	0.0889	0.0907	0.0949	0.0997
10	156.25	4096	0.0829	0.087	0.0912	0.0933
11	206.25	4096	0.0791	0.084	0.0882	0.092
12	256.25	4096	0.0785	0.0838	0.0885	0.0914

13	306.25	4096	0.08	0.0853	0.0904	0.0925
14	406.25	4096	0.0844	0.0896	0.094	0.0945
15	506.25	4096	0.0897	0.094	0.0974	0.0968
16	656.25	4096	0.0956	0.098	0.0987	0.0957
17	806.25	4096	0.099	0.0978	0.0945	0.0878
18	905.25	4096	0.099	0.0945	0.088	0.0793
19	1006.25	4096	0.0968	0.0891	0.0784	0.0654
20	1106.25	4096	0.0926	0.0801	0.0661	0.0502
21	1256.25	4096	0.0829	0.0653	0.0433	0.0213
22	1506.25	4096	0.0594	0.0325	0.01	0.0303
23	1756.25	4096	0.0325	0.01	0.0402	0.0754
24	2006.25	4096	0.01	0.0265	0.062	0.0977

Table 3 Measurement parameters including excitation frequency and excitation voltage for each top mass

Measurements at RISE were performed at three different shaker systems at fixed frequencies and with frequency sweeps up to 1 kHz. Each transducer was loaded with various top masses and accelerations.

Evaluation:

Time domain measurement data are used to investigate the transducer sensitivity degradation over the frequency. Levenberg-Marquardt algorithm LMA is implemented in Python3 to solve non-linear least squares sine fit [5, 6] and to determine the amplitude and the phase of the recorded force and acceleration signals. A simple Fast Fourier transform FFT feeds LMA to initialize amplitude and phase. Figure 47 and Figure 48 show the code implemented in Python3 to signal characterization and corresponding results respectively.

DOI 10.5281/zenodo.7113187

```python
ch_sinfit = 3                                          # Number of channels to apply the sinfit
i=0
res=dict()
all_xfit = np.zeros(shape=(Ns,))                       # Define a zero array in order to using in vstack function
for j in range (0,Np):
    for i in range (0,ch_sinfit):
        def fit_sin(tt,yy):
            tt = pd.Series(T).array
            yy = pd.Series(sli[(i*Np)+j]).array
            ff = np.fft.fftfreq(len(tt) , deltaT)          # Returns the DFT samle freuencies
            Fyy = abs(np.fft.fft(yy))
            guess_freq = abs(ff[np.argmax(Fyy[1:])+1])     # Excluding the zero frequency (offset)
            guess_amp = np.std(yy)*math.sqrt(2)
            guess_offset =np.mean(yy)
            guess = np.array([guess_amp, 2. *np.pi*guess_freq, 0., guess_offset])

            def sinfunc(t, A, w, p , c): return A * np.sin(w*t+p)+c
            popt, pcov = scipy.optimize.curve_fit(sinfunc, tt, yy, p0=guess)
            A , w , p , c = popt
            f = w/(2.*np.pi)
            fitfunc = lambda t: A*np.sin(w*t+p)+c
            return {"amp":A, "phase": p, "offset":c, "freq.":f , "fitfunc":fitfunc , "maxcov":np.max(pcov), "rawers" :(guess,popt
        res[(ch*j)+i] = fit_sin(T, sli[(i*Np)+j])
        xfit = res[(ch*j)+i]["fitfunc"](T)
        all_xfit = np.vstack((all_xfit,xfit))
all_xfit = all_xfit[1:,:]                          # Remove the zero array
```

Figure 47 code written in Pyhon3 to perform LMA and determining amplitude and phase of the signal in the time domain

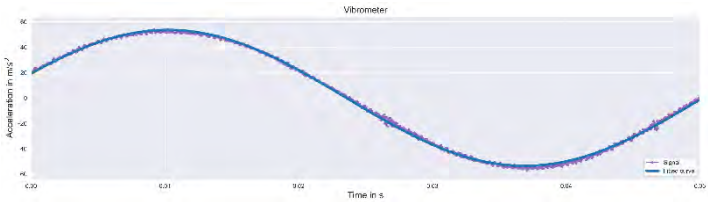

Figure 48 Acceleration signal recorded by laser scanning vibrometer and its non-linear LM sine fit

Measurement results:

sinusoidal dynamic calibration procedure according to the guideline DKD 3 – 10 sheet 2 [7] is utilized to define the internal mass and dynamic sensitivity of the force transducer as described below.

Internal mass

Internal mass or head mass m_i of the force transducer (see Figure 42) is calculated as a part of dynamic response characterization. By the creation of the ratio between the force transducer output signal and the measured acceleration on the top mass, the internal mass can be calculated according to equation (4):

$$\left(\frac{U_f}{a_t}\right)_0 = S_{f0}.m_t.K_0 + S_{f0}.m_i + S_{f0}.m_a \qquad (4)$$

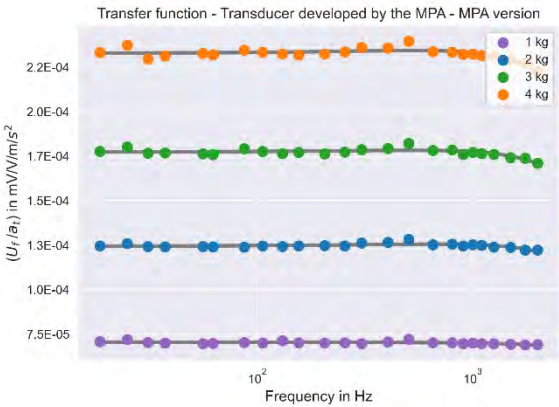

Figure 49 Transfer function as the ratio between the transducer output signal and acceleration on the top mass

where $\left(\frac{U_f}{a_t}\right)_0$ is the transfer function extrapolated to zero frequency using polynomial regression. A function of second order is used to find a line of best fit to measurement data for each mass (see Figure 49).

DOI 10.5281/zenodo.7113187

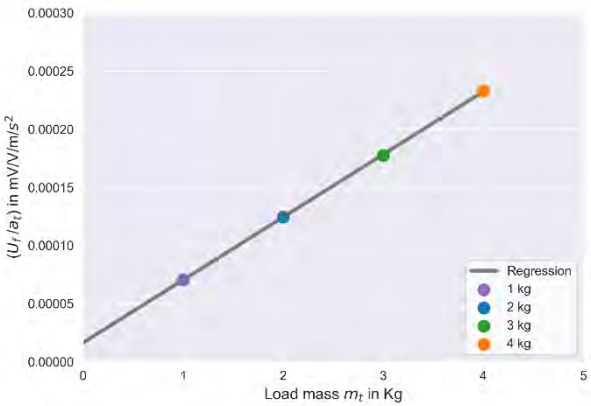

Figure 50 determination of the force transducer internal mass using transfer function

Figure 50 illustrates intercepts of the transfer function shown in Figure 49 calculated by the extrapolation to zero frequency over four top masses. By using linear regression, the intercept of the fitted line is calculated. The resulting internal mass calculated with this method for the strain gauge transducer selected for this validation report is equal to 0.259 kg.

Using the method described above RISE has determined the internal mass of three the transducers used in measurements to be:
13.28 g for PCB 208C05 (overall transducer's mass 24.32 g)
0.15 kg for HBM / 5 kN (overall transducer's mass 1.2 kg)
2.59 kg for HBM / 50 kN (overall transducer's mass 10 kg)

This method, especially in case of small internal masses, might lead to deviating results, giving even negative mass values [7] .

Dynamic sensitivity of force transducer

Figure 51 illustrates the sensitivity reduction of the force transducer under dynamic conditions stated separately for each mass in the frequency range outlined in Table 3.

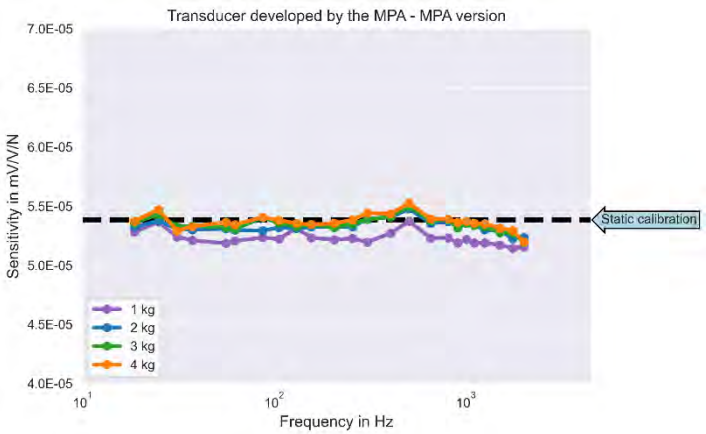

Figure 51 Sensitivity of the force transducer developed by MPA Stuttgart measured under dynamic conditions

DOI 10.5281/zenodo.7113187

The calculated internal mass m_i, the mass of all mechanical adapters above the sensing element m_a and dynamic behaviour of the amplifier are taken to account. The dashed line in Figure 51 represents the Static sensitivity S_{f0}. As can be seen the dynamic sensitivity for different mass differ slightly and exhibit a reduction up to more than 5%.

For transducers selected at RISE the observed dynamic sensitivity S_f related to the static S_{f0} is as follows:

up to 5 % difference for PCB 208C05
up to 3 % difference for HBM / 5 kN
up to 7 % difference for HBM / 50 kN

Figure 52 shows an example of measured dynamic sensitivity combined from three frequency sweep tests.

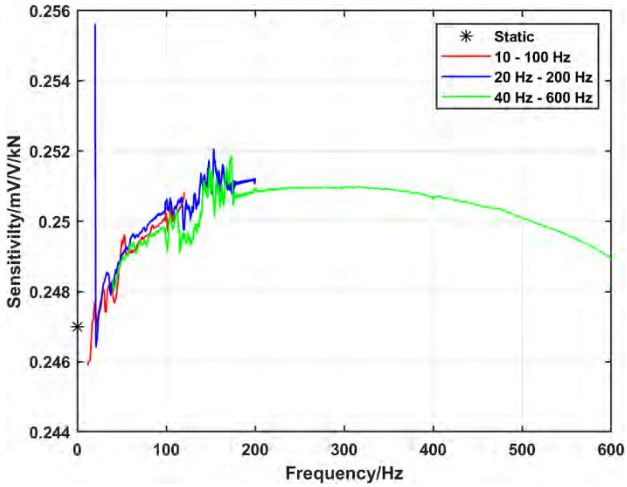

Figure 52 Dynamic sensitivity of the HBM / 5 kN transducer

System Identification:

Parametric identification of the force transducer to define the stiffness and the damping coefficient needed for the above-mentioned model is part of the calibration process. However, the precise and stable definition of these parameters has been always challenging. In this report, the well-established approach based on sinusoidal calibration according to the guidelines DKD 3-10 [7] in part1 (Frequency domain) is followed by two new approaches for the

DOI 10.5281/zenodo.7113187

investigation of the model parameters in the time domain in part2.

Frequency Domain

The model parameters including stiffness k_f and damping b_f (see Figure 42) are also defined in order to the force transducer characterization under dynamic conditions. In this regard, the ratio between acceleration on the load mass and acceleration on the shaker must be created.

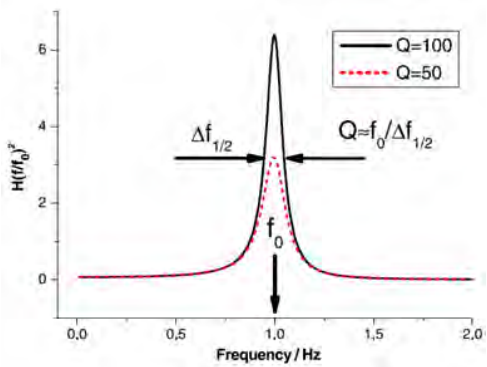

Figure 53 ratio of the acceleration of the top mass and shaker table

Figure 53 illustrates the amplitude response of the system, where f_0 is resonance frequency.

Stiffness:

By calculating f_0 and considering the internal mass of the transducer m_i, the stiffness of the force transducer can be calculated using equation (5)

$$K_f = (2\pi . f_0)^2 . [m_\mathrm{a} + m_\mathrm{i} + (m_\mathrm{t} \cdot K_0)] \qquad (5)$$

Damping:

The ratio between the full width at half maximum of the resonance curve Δf and the resonance frequency f_0 defines the quality factor Q. An uncertainty contribution below 0.1% can be achieved by a value of above 20 for the quality factor. The damping coefficient is given by equation (6):

$$\begin{aligned} b_f &= \frac{\Delta f}{f_0} \sqrt{k_f . [m_\mathrm{a} + m_\mathrm{i} + (m_\mathrm{t} \cdot K_0)]} \\ &= \frac{1}{Q} \sqrt{k_f . [m_\mathrm{a} + m_\mathrm{i} + (m_\mathrm{t} \cdot K_0)]} \end{aligned} \qquad (6)$$

Time Domain

Evaluation of measurement data in the time domain instead of the frequency domain can be advantageous because of the raw data access and therefore preventing some transformation errors such as spectral leakage. Furthermore, high fluctuations in the defined damping coefficient and unstable model parameters are reported by

DOI 10.5281/zenodo.7113187

independent research groups [8, 9] which encourage further investigations and the utilization of modern tools.

The following two methods are introduced using time-domain measurement data in order to define the damping and stiffness of force transducers.

ARMAX and BJ Models

As an alternative to sinusoidal calibration a new measurement and evaluation method is proposed by the PTB utilizing periodic chirp to excite the electrodynamic shaker [10]. The axial acceleration measurement in combination with the evaluation of the measurement data in the time domain using ARMAX and Box-Jenkins results in stable parameters definition.

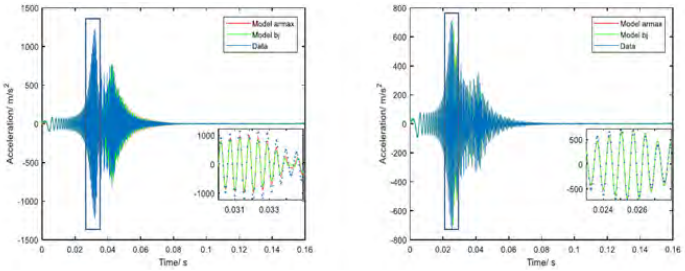

Figure 54 Experimental data and model fit of acceleration with 2kg (left) and 4 kg (right) top mass

Deep Learning Models

As the second approach for the evaluation of the measurement data in the time domain and the determining model parameters, a novel method based on leveraging artificial intelligence AI is proposed by the PTB which can pave the path for the digitalization of the calibration

process. Same as the method introduced in the last section, periodic chirp calibration is used to perform measurements. Unlike that approach Laser interferometer (Polytec PSV-400) is used for both the acceleration measurements on the top mass and on the bottom at several points.

The main idea is to learn a general mode for the acceleration on each surface and the utilizing nonlinear character of the deep neural networks DNN to filter anomalies in the recorded signal arising from nonsymmetric effects including the rocking (tilt) motion of calibration setup as the main dominant source of uncertainty in the acceleration and hence force and other parasitic effects.

Four different types of deep neural network DNN [11] namely, Recurrent Neural Network RNN, Long Short-Term Memory LSTM [12], Gated Recurrent Unit GRU [13] and Bidirectional RNN [14] are suggested which are able to learn a model of sequence data recorded in the time domain.

Figure 55 schematically shows the sequential acceleration measurement on the circular plate and load mass at 16 and 24 points respectively.

DOI 10.5281/zenodo.7113187

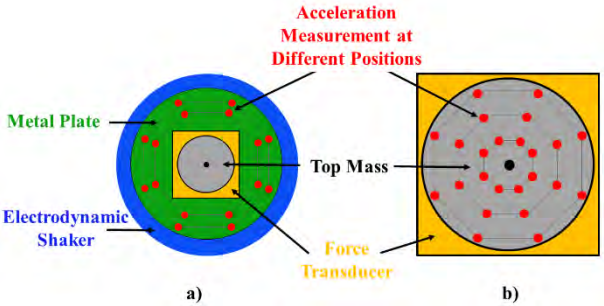

Figure 55 Setup top view – Acceleration measurement at different points a) on the plate all around the transducer b) on the top mass

The performing acceleration measurement at several points yields a good understanding of the rocking (tilt) movement of the calibration setup which in turn provides a data set that can be fed to the different DNN architectures. However, a point-by-point investigation must be performed before the training of the DNN can be started. For this purpose, two sets of investigations are carried out at PTB in the time and frequency domain.

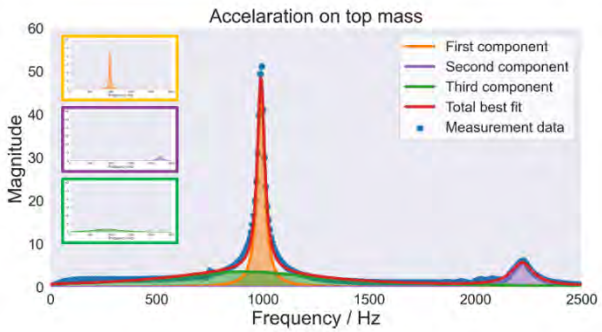

Figure 56 Best fit results as a linear mixture of three Lorentzian functions

Figure 56 shows in frequency domain representation of the recorded acceleration signal for one point on the top mass. The Lorentzian function is used to characterize this signal. The best results reach when the fitting model is considered as a linear mixture of three Lorentzian functions with different parameters. While the first peak (shown in orange) and the second peak (shown in purple) represent the resonance of the setup and shaker respectively, the third peak (wide and small green peak) can be put down to a parasitic effect or another degree of freedom. However, in further investigation, just the first peak is characterized by its FWHM and height for all points on the top mass and on the mechanical adapter. Figure 57 and Figure 58 show a comparison for all points on these two surfaces respectively.

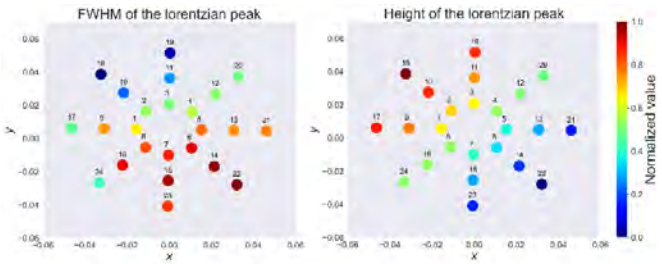

Figure 57 Comparison of the FWHM and height of Lorentzian function at different points on the top mass

DOI 10.5281/zenodo.7113187

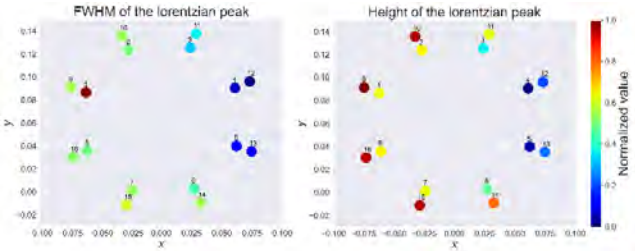

Figure 58 Comparison of the FWHM and height of Lorentzian function recorded at different points on the metal plate

As it can obviously be seen there is a dramatic deviation in FWHM and the height of the Lorentzian function on both surfaces. Furthermore, one can easily distinguish between two areas on the top mass where the fitting model outputs in one area, wide and short peaks, and in the other one, narrow but tall peaks but there are no such distinguishable areas on the metal plate.

Thus, averaging the acceleration over all the points on surfaces would be a bad idea because of the asymmetry and the dissimilarity observed here.

It should be noted that the first set of investigations are susceptible to some errors arising from the FFT and the fitting model initialization. Therefore, in the second set of investigations and in the time domain, the average acceleration values for every surface (top mass and metal plate) are used as a reference. The relative deviation is calculated by taking the Root Mean Squared Error (RMSE) metric.

This method serves as a common-sense approach (non-deep learning baseline) that will be used to demonstrate the superiority of the black-box deep learning-based method

and yields a good understating of the anomaly distribution in training data. A detailed explanation of the method represented in this report along with a short introduction to deep neural networks mentioned in this report can be found in the paper submitted by the PTB on IMEKO TC3 – 2022 [15].

DOI 10.5281/zenodo.7113187

Temperature effects

The temperature can affect significantly results of dynamic calibration of the force transducer. Generally, even in the controlled room, a working shaker generate heat which can be then transferred to the measuring equipment. RISE has concluded that the amount of thermal energy transferred from the shaker depend mostly on the effectiveness of the cooling system of the shaker (if any). Temperature measurements of the transducer's body with K-type thermocouples allowed to observe that the heat transfer is significantly lower for shakers having their own cooling system.

Another effect to be considered is the temperature change of the transducer's elastic element subjected to periodic stresses of high frequency. A study of this effect requires however temperature measurement directly on the elastic element.

Conclusion

The proposed model for the dynamic sensitivity of a force transducer can be used to evaluate the dynamic calibration with periodic forces. It has however some boundaries, such as assumption that the adaptation parts as very stiff (b_c/k_c close to zero). For another assumption that the spring element of the transducer is also stiff (small b_f/k_f), the dynamic sensitivity can be described by a function of angular frequency ω (the sensitivity decreases with the square of ω). This approximation can fail depending on the measurement setup and the quality of the periodic excitation which both can significantly influence the transfer function used to convert time-dependent signals to the frequency domain (commonly FFT).

While it is relatively easy to perform the dynamic calibration, the evaluation of measurement data remains to be a hard task.

More information about the dynamic measurement of force can be found in literature survey [16]

DOI 10.5281/zenodo.7113187

Uncertainty analysis of the parametric identification:

Along with other uncertainty contributions arising from equipment, model parameters and experiment, utilizing each of the above-mentioned methods for the system identification is associated with the introduction of a new contribution to uncertainty shown as the identification techniques in the diagram below.

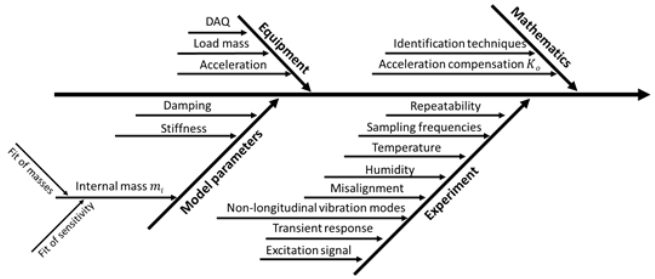

Figure 59 Ishikawa diagram of the influences on a dynamic calibrated force transducer

Parameters

The dynamic calibration of a force transducer allows determination of several parameters. A method for estimating the measurement uncertainty of these parameters is described below.

Internal mass

The determination of internal mass of the transducer is based on:

1. Extrapolation of the transfer function to zero frequency $\left(\frac{U_f}{a_\mathrm{t}}\right)_0$ for each top mass m_t
2. Linear fit of $\left(\frac{U_f}{a_\mathrm{t}}\right)_0$ values as a function of m_t

Each of these two steps give a separate uncertainty contribution, u_extrapol and u_lin respectively. Even though it is not an easy task, the uncertainty contribution due to transfer function analysis $u_\mathrm{transfer.fun}$, if possible, needs also to be estimated. Evaluation of the combined uncertainty of the internal mass determination u_{m_i} shall consider correlations. Assuming a special case where all the input estimates are strongly correlated $r(x_\mathrm{i}, x_j) = +1$ [15], $u_c(m_\mathrm{i})$ can be expressed as follows:

$$u_{m_\mathrm{i}}^2 = \left(c_1 \cdot u_\mathrm{extrapol} + c_2 \cdot u_\mathrm{transfer.fun} + c_3 \cdot u_\mathrm{lin}\right)^2 \qquad (7)$$

Standard uncertainties correspond to the standard deviations of the mathematical operations, whereas sensitivity coefficients c_1, c_2, c_3 depend on applied functions.

Dynamic sensitivity

According to [7] , the measurement uncertainty of the dynamic sensitivity S_f can be obtained using regression

DOI 10.5281/zenodo.7113187

parameters of the function $S_f(\omega)$. This uncertainty u_{S_f} is a function of angular frequency ω.

Another method can consider using practical model in a similar way as in Part A of this report. This results in the following equation:

$$F_{\mathrm{dyn}}(f) = \frac{U_f}{S_f} \prod_{i=1}^{N} K_i \qquad (8)$$

where K_i represent correction factors or acceleration compensation depicted in Figure 59.

Stiffness

Measurement uncertainty of stiffness parameter, given by (9), can be evaluated according to GUM [17] .

Damping

Measurement uncertainty of damping parameter, given by (10), can be evaluated according to GUM [17].

Deep neural networks DNN

Deep neural networks DNN allow the understanding of complex scientific relationships because of their nonlinear structure. However, their black-box character barricades a trustworthy uncertainty quantification. At the end of this

report, three methods including Bayesian neural networks [18, 19], dropout-based methods [20, 21], and ensemble techniques [22] are motivated as possible further work to quantify DNN uncertainty.

DOI 10.5281/zenodo.7113187

References

[1] „Metallic Materials – Calibration of Force-Proving Instruments Used for the Verification of Uniaxial Testing Machines ISO 376,“ *International Organization for Standardization: Geneve, Switzerland,* 2011.

[2] M. Kobusch, S. Eichstädt, L. Klaus und T. Bruns, „Investigations for the model-based dynamic calibration of force transducers by using shock excitation,“ *IMEKO 22nd TC3, 12th TC5 and 3rd TC22 International Conference vol 4 Cape Town, Republic of South Africa,* pp. 45-51, 2014.

[3] R. Kumme, „Investigation of a primary method for a dynamic calibration of force measuring instruments: a contribution to reduce the measuring uncertainty,“ *Doctoral Thesis TU Braunschweig, PTB-Bericht MA-48,* 1996.

[4] N. Vlajic und A. Chijioke, „Traceable dynamic calibration of force transducers by primary means,“ *Metrologia,53A136-48,* 2016.

[5] K. Levenberg, „A method for the solution of certain non-linear problems in least squares,“ *Quarterly of Applied Mathematics.,* 1944.

[6] D. Marquardt, „An Algorithm for Least-Squares Estimation of Nonlinear

Parameters,“ *SIAM Journal on Applied Mathematics,* 1963.

[7] „Dynamic calibration of force transducers according to the sinusoidal method,“ *Guideline DKD-R 3-10 Sheet 2,* 2019.

[8] C. Schlegel, G. Kieckenap, B. Gloeckner, A. Buß und R. Kumme, „Traceable periodic force calibration,“ 2012.

[9] A. Chijioke und N. Vlajic, „PRIMARY SINUSOIDAL CALIBRATION OF FORCE TRANSDUCERS UP TO 2 KILOHERTZ,“ *XXI IMEKO World Congress,* 2015.

[10] S. Hassan, C. Schlegel, R. Kumme und R. Tutsch, „Parametric identification of dynamic force transducer,“ *Journal of Physics,* 2018.

[11] T. Qin, Deep Learning Basics, Springer Singapore.

[12] S. Hochreiter und J. Schmidhuber, „Long Short-Term Memory,“ *Neural Computation 9,* p. 1735–1780, 1997.

[13] K. Cho, B. Merrienboer und D. Bahdanau, „On the Properties of Neural Machine Translation: Encoder–Decoder Approaches,“ 2014.

[14] M. Schuster und K. Paliwal, „Bidirectional Recurrent Neural Networks“, IEEE Transactions on signal processing,“ *IEEE Transactions on signal*

DOI 10.5281/zenodo.7113187

processing, Bde. %1 von %245, no. 11, 1997.

[15] D. Mirian, R. Kumme und R. Tutsch, „FIRST STEPS TOWARD LEVERAGING ARTIFICIAL INTELLIGENCE FOR PRECISE CHARACTERIZATION OF FORCE TRANSDUCERS," *IMEKO TC3,* 2022.

[16] J. Hjelmgren, „Dynamic measurement of force - A literature survey," p. 46, 2002.

[17] „JCGM 100:2008 Evaluation of measurement data — Guide to the expression of uncertainty in measurement," 2008.

[18] I. Kononenko, „Bayesian Neural Networks," *Biological Cybernetics 9 Springer-Verlag,* 1989.

[19] J. Yao, W. Pan, S. Ghosh und F. Doshi-Velez, „Quality of Uncertainty Quantification for Bayesian Neural Network Inference," 2019.

[20] Y. Gal, J. Hron und A. Kendall, „Concrete Dropout," *Conference on Neural Information Processing Systems NIPS,* 2017.

[21] D. P. Kingma, T. Salimans und M. Welling, „Variational Dropout and the Local Reparameterization Trick," *Advances in Neural Information Processing Systems.*

[22] T. G. Dietterich, Ensemble methods in machine learning, International Workshop on Multiple Classifier Systems: Springer.

DOI 10.5281/zenodo.7113187

The content presented was developed within the framework of the EU-funded project ComTraForce " Comprehensive traceability for force metrology services " *with the* support of international partners from science and industry.

https://www.ptb.de/empir2019/comtraforce

The EMPIR initiative is co-funded by the European Union's Horizon 2020 research and innovation programme and the EMPIR Participating States